SAPIENZA
Università di Roma
Facoltà di Farmacia e Medicina

Ph.D. in
MORPHOGENESIS AND TISSUE ENGINEERING

XXXIII Cycle
(A.A. 2019/2020)

MOLECULAR AND CELLULAR NETWORKS DRIVING NEUROGENIC MUSCLE ATROPHY

Ph.D. Student
Daisy Proietti

Tutor
Dr. Luca Madaro

Coordinator
Prof. Antonio Musarò

Index

1. SUMMARY

During neurogenic muscle atrophy, the interruption of transmission of neurogenic signals to muscle, caused by loss the of neuromuscular junction (NMJ) integrity, leads to muscle atrophy, an event that causes loss of muscle functionality with the obvious deleterious outcomes. NMJs degeneration is a prominent aspect of denervation, aging, and some pathological conditions, such as Amyotrophic Lateral Sclerosis (ALS). The precise molecular mechanisms and roles of muscle-resident cells, during neurogenic muscle atrophy, remain largely unknown. Availableevidence suggests that the effect on myofibers caused by neuron loss involves neighboring resident cells. Therefore, we analyzed the gene expression profiles at bulk and single-cell level of Itga7-expressing cells in muscle and revealed the existence of a subpopulation of muscle-resident glial cells, distinct from muscle satellite cells, that are selectively activated upon nerve injury. Upon nerve lesion, these cells expand and activate a neurotrophic program, that is turned off upon recovery of NMJ integrity. Moreover, in a mouse model of ALS, these muscle-resident glial cells increase during disease progression but exhibit impaired neurotrophic activity, suggesting that defective activation of glial cells could be implicated in ALS pathogenesis. Therefore, a better understanding of the cellular and molecular signaling pathways in muscle-resident cells during traumatic or pathological denervation is critical for developing better therapies against neurogenic muscle atrophy and degenerative diseases such as ALS.

2. INTRODUCTION

2.1 The skeletal muscle: a brief overview

Skeletal muscle is one of the most dynamic and plastic tissues of the human body. In humans, skeletal muscle comprises approximately 40% of body weight. In physiological conditions, a balance between the biosynthetic and catabolic systems maintains muscle mass. Several factors, such as nutritional status, hormonal balance, physical exercise, and injury or disease, alter this balance causing the predominance of one system over the other, and leading to either muscle hypertrophy or atrophy (Frontera and Ochala, 2015).
Skeletal muscle is able to generate force, allows body movement, contributes to body temperature regulation, and repairs itself when needed. Skeletal muscle is composed of long multinucleated, post-mitotic, cells called muscle fibers (myofibers) packed with contractile myofibrils that entirely fill the cytoplasm pushing the multiple nuclei against the cell membrane, the sarcolemma. The muscle fibers are the basic contractile units of skeletal muscles. These fibers are surrounded by a connective tissue sheath called the *endomysium*. Groups of fibers are arranged in bundles and surrounded by another layer of connective tissue known as the *perimysium*. Several bundles of aligned muscle fibers form the skeletal muscle, which is further enveloped by a connective sheath, the *epimysium*. The connective layers (epimysium, perimysium, and endomysium) merge into a single organization to make contact with one or more fixed bone points. As well as being rich in connective tissue, the skeletal muscle is highly vascularized and innervated to provide essential supply and nutrients for muscle function (Figure1) (Chargé and Rudnicki, 2004; Yusuf and Brand-Saberi, 2012).

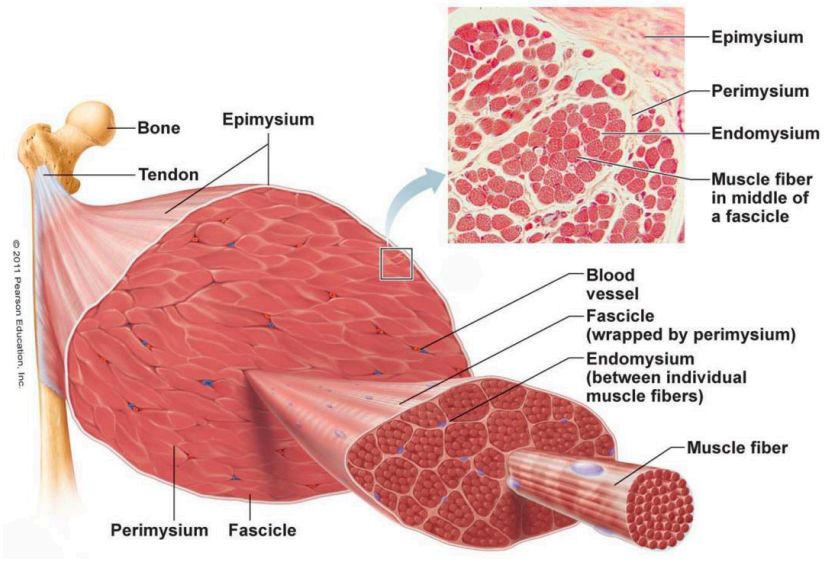

Figure 1 Schematic representation of the structure of skeletal muscle. (Pearson Education. Inc. 2011)

Other cellular elements in the sarcoplasm of muscle fibers include a transverse tubular system (T tubule), the sarcoplasmic reticulum, and a mitochondrial network; the exact amount of these elements may depend on the fiber type (Chal and Pourquié, 2017; Frontera and Ochala, 2015). Skeletal muscle fibers can be classified in 4 subtypes: one type of slow-twitch fiber (type I) and three types of fast-twitch fibers (type IIa, type IIx/d, and type IIb), of which type I and type IIa fibers are oxidative, whereas type IIx and type IIb fibers are primarily glycolytic (Schiaffino and Reggiani, 2011). The proportion of each fiber type within a muscle determines its overall contractile property. Despite having different physiological properties, the basic mechanism of muscle contraction is similar in all myofiber types and is the result of a "sliding mechanism" of the myosin-rich thick filament over the actin-rich thin filament after neuronal activation (Chargé and Rudnicki, 2004; Schiaffino and Reggiani, 2011).

2.2 Muscle-Resident Cell Populations (Single-Cell Analysis)

In addition to myofibers, skeletal muscle is composed of a large and heterogeneous assortment of cell populations, including muscle stem cells, motor neurons, endothelial cells, immune cells, fibro/adipogenic progenitors (FAPs), that interact with each other to maintain muscle homeostasis and orchestrate regeneration (Figure2) (Bentzinger et al., 2013; Collins et al., 2005; Farup et al., 2015).
Among these cells, muscle satellite cells (MuSCs) are the bonafide muscle stem cells that express the transcription factor *Pax7* and are located beneath the muscle basal lamina. These cells exist in a quiescent state during homeostasis in adult tissues and become activated in response to acute muscle damage or chronic degenerative conditions (Brack and Rando, 2012; Feige et al., 2018; Wosczyna and Rando, 2018). Upon injury, MuSCs become activated, proliferate, differentiate, and fuse to repair damaged myofibers. The activation of MuSCs is controlled by specific transcription factors named Myogenic Regulatory Factors (MRFs) such as Myf 5, MyoD, Myogenin and MFR4. In addition to cell proliferation and myofiber differentiation, activated MuSCs also have an important function in maintaining their own satellite cell reserve pool through self-renewal, which is essential for continuous muscle regeneration. It is regulated by different signaling pathways, such as Notch, Six1 and STAT3 (Le Grand et al., 2012; Tierney et al., 2014; Wen et al., 2012; Zhu et al., 2016). However, the appropriate responses of MuSCs to injury depends on both resident and infiltrating cells. For example, upon muscle injury, FAPs become activated, proliferate and expand, and release paracrine factors to promote MuSCs-mediated regeneration (Biferali et al., 2019; Heredia et al., 2013; Joe et al., 2010; Mozzetta et al., 2013; Wosczyna et al., 2019). However, as regeneration proceeds, FAPs are cleared from the regenerative niche by apoptosis (Lemos et al., 2015) and failure in doing so has been associated with their pathological accumulation and with several muscle dysfunctions. Indeed, in conditions of chronic injury, such as in degenerating

dystrophic muscles, FAPs mediate fibrotic and fat tissue deposition, disrupting the environment necessary for muscle regeneration.
Complete muscle repair is also dependent on two different subtypes of macrophages: pro-inflammatory (M1) and anti-inflammatory (M2) macrophages. Through timely balanced pro- and anti-inflammatory waves, they regulate FAPs function and fate, which in turn determine the regeneration outcome, based on the stimulation of MuSCs and transient or permanent deposition of extracellular matrix (ECM) (Muñoz-Cánoves and Serrano, 2015).

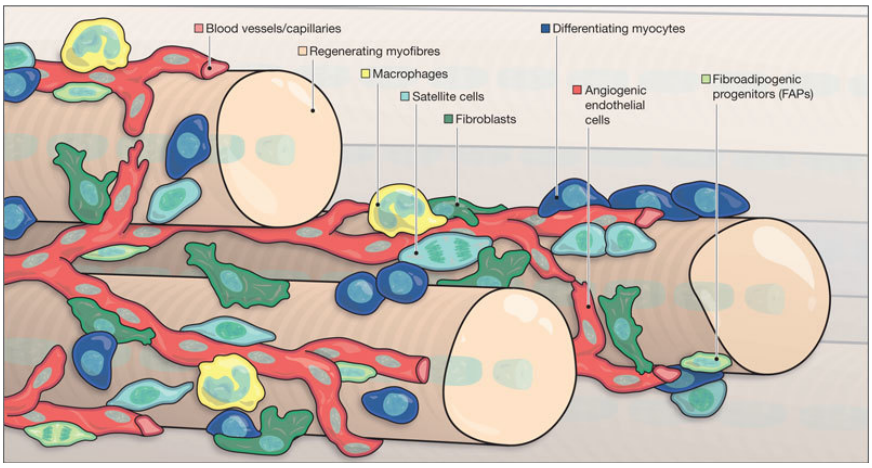

Figure 2 Schematic representation of muscle resident cell types. (Bentzinger et al., 2013)

Despite many studies describing the existence of a complex regulatory network between myofibers and muscle resident cells, the characterization of the distinct cell types within skeletal muscle at the single-cell level has become possible only recently through Single-cell RNA-sequencing (scRNA-seq). This technique provides the opportunity to dissect individually heterogeneous mononuclear cells resident in tissue, based on their transcriptomic profiles (Hwang et al., 2018; Zeng and Dai, 2019).
Previously, bulk RNA-seq technologies have been widely used to study gene expression patterns at the cell population level, however, these techniques mainly reflect the averaged gene expression across

thousands of cells. The advent of scRNA-seq, instead, has allowed us to explore gene expression profiles at the single-cell level, opening up new frontiers of research, such as the study of complex and rare cell populations or the regulatory relationships between genes, as well as lineage tracing during development. Although various scRNA-seq technologies have been developed in recent years, the scRNA-seq protocol provides some common steps:

- Single-cells isolation (several different approaches are available for isolating single cells, including limiting dilution, micromanipulation, flow-activated cell sorting (FACS), laser capture microdissection (LCM), and microfluidics).
- Cell Lysis (cells are lysed in a hypotonic buffer)
- Reverse Transcription for cDNA synthesis (the mRNAs are captured by poly(A)+ selection, using poly(dT) primers).
- Amplification of cDNA using conventional PCR or in vitro transcription.
- Sequencing (at the moment, most protocols use the Illumina platform).

A recent strategy for improving the quantitative nature of scRNA-seq has been to use unique molecular identifiers (UMIs), which barcode each individual mRNA molecule within a cell during reverse transcription. Sequenced reads that arise from PCR-duplicated tags will have the same random barcode sequence (Kolodziejczyk et al., 2015).

However, the scRNA-seq has some inherent limitations, including the use of a low number of cells, sensitivity to sample preparation methods, high prevalence of dropout events (some specific transcripts cannot be detected), bias of transcript coverage, low capture efficiency, and sequencing coverage, resulting in scRNA-seq data with a higher level of technical noise than bulk RNA-seq data. Accordingly, quality control (QC) of scRNA-seq data is crucial in order to identify and remove the low-quality data to get robust and reproducible results and avoid artifacts in data interpretation. For instance, those samples containing only a few numbers of reads should be discarded. Tools initially developed for

QC of bulk RNA-seq data, such as FastQC1, can also be employed to check the sequencing quality of scRNA-seq data. Moreover, after reads alignment, samples with a very low mapping ratio should be eliminated because they contain massive unmappable reads that might have resulted from RNA degradation (Chen et al., 2019). These are just a few examples of how we can increase the quality and reliability of scRNA seq data. Regardless, RNA seq is a technology, that has greatly revolutionized and facilitated biological and clinical research.

Recent scRNA-seq studies conducted on mouse hindlimb muscle have characterized the cellular diversity of the skeletal muscle (Dell'Orso et al., 2019; Giordani et al., 2019; De Micheli et al., 2020; Oprescu et al., 2020). In these studies, myogenic progenitors, containing MuSCs myoblasts myocytes and/or myofibers, and multiple non-myogenic cell populations, including FAPs, tenocytes, smooth muscle cells (SMCs), mesenchymal progenitors, endothelial cells, neuro-muscular cells, and different immune cell populations were annotated. In Giordani's work, for example, two understudied populations were identified: smooth muscle mesenchymal cells (SMMCs) and interstitial tenocytes (Giordani et al., 2019); others scRNA-seq studies, instead, defined distinct transcriptional programs in quiescent and activated muscle resident cells during muscle regeneration (MuSCs, FAPs and immune cells), describing spatiotemporal dynamics in gene expression, pseudotime trajectories, population composition, and cell-cell interactions (Dell'Orso et al., 2019; De Micheli et al., 2020; Oprescu et al., 2020). scRNA-seq is revolutionizing our fundamental understanding of the heterogeneity of muscle resident cells in homeostatic and pathological conditions and their dynamic changes in response to perturbations. The scRNA-seq approaches, indeed, represent a powerful tool to identify the signature of a small number of cells within the pool of cells analysed. These studies could open up new frontiers of research which may lead to new therapeutic strategies to counteract the neuromuscular diseases.

2.3 The Neuromuscular Junction

A motor neuron and the skeletal muscle fibers innervated by that motor neuron's axonal terminals constitute a motor unit. The motor neuron's axonal terminal is divided into thin demyelinated branches. Each branch forms numerous expansions called synaptic buttons located in a specialized region of the muscular membrane called the motor endplates. Here, the interactions between nerve cells, muscle cells and synapse-associated glial cells, also called Perisynaptic Schwann Cells (PSCs), form the chemical synapse of the neuromuscular junction (NMJ).
Upon the arrival of action potentials in chemical synapses, the motoneuron terminals release acetylcholine (ACh), which activates the ACh receptors (AChRs) on muscle fibers to depolarize the muscle cell and trigger calcium release from the sarcoplasmic reticulum to initiate muscle contraction (Li et al., 2018).
Neuromuscular junction formation, development and maintenance require extensive communication among the three components of the synapse: presynaptic motoneurons, postsynaptic muscle fibers, and PSCs. (Figure3)(Lepore et al., 2019; Li et al., 2018). For example, nerve terminals secrete positive factors, such as agrin, to induce the AchRs clustering on the muscle surface playing an important role in NMJ formation and maintenance: indeed, NMJs disintegrate in mice that lose some of these factors, such as agrin or CLIPR-59 (Barik et al., 2014; Couesnon et al., 2013; Eguchi et al., 2016; Kummer et al., 2006; Samuel et al., 2012). In turn, the skeletal muscle is a source of signals that influence the development, survival and maintenance of the motor neurons. Indeed, in the absence of skeletal myogenesis in mice lacking the transcription factors Myf5 and MyoD, all somatic motor neurons are eliminated by apoptosis (Kablar and Rudnicki, 1999). Likewise, ablating PSCs impairs the synaptic function, whereas the ultrastructure of nerve–muscle contacts, are not significantly affected (Feng and Ko, 2008; Koirala et al., 2003; Lin et al., 2000; Reddy et al., 2003).
Neuromuscular junctions degeneration is a prominent aspect of denervation, aging, and pathological conditions, such as

Amyotrophic Lateral Sclerosis (ALS) (Cappello and Francolini, 2017; Chai et al., 2011; Valdez et al., 2010).

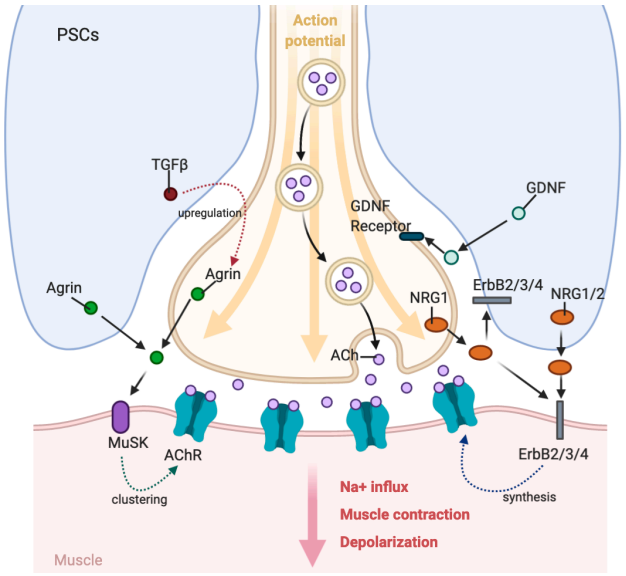

Figure 3 Schematic representation of NMJ.

2.4 Schwann Cells: Peripheral Glial Cells

The Schwann cells (SCs) play a critical role in maintaining the peripheral nervous system (PNS), through their myelinating function and their role in nerve pathology and repair. There are two types of Schwann cells: myelinating and non-myelinating. Non-myelinating Schwann cells can be subdivided into Remak cells, which ensheath unmyelinated axons along their length (Remak fibers), and terminal or perisynaptic Schwann cells (PSCs), which are located on axon terminals at the neuromuscular junction (Figure 4) (Griffin and Thompson, 2008; Verkhratsky and Butt, 2013).

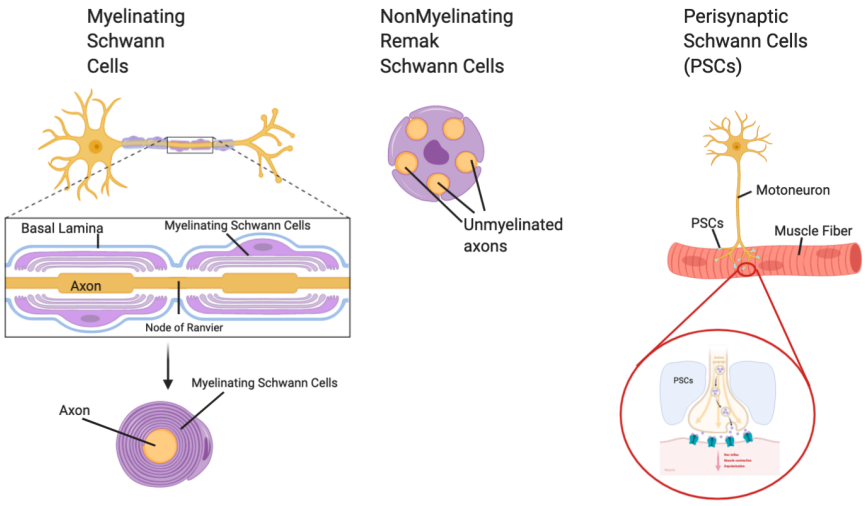

Figure 4 Schwann cell subtypes.

Myelinating SCs provide the myelin ensheathment of all large-diameter peripheral axons. Each myelinating SC associates with a single axon. Consecutive Schwann cell myelin internodes are separated by nodes of Ranvier, the site of action potential propagation: the action potential jumps from node to node, in a process called saltatory conduction. Indeed, myelination greatly increases the speed of conduction of nervous impulses along axons and saves energy.

Non-myelinating Remak Schwann cells ensheath multiple small-caliber axons (< 1 mm diameter). (Taveggia et al., 2005). These small axons include the C fiber nociceptors, the postganglionic sympathetic fibers, and some of the preganglionic sympathetic and parasympathetic fibers. Individual Remak Schwann cells promiscuously ensheath both sensory and sympathetic axons. These cells are important for structural and trophic support for axons. For instance, they produce glial derived neurotrophic factor (GDNF) and Nerve Growth Factor (NGF), and are important for ion homeostasis, such as potassium regulation (Robert and Jirounek, 1994). Remak Schwann cells specifically express a1b1 and a7b1 integrins, which

are essential for interactions with laminin in the basal lamina (Yu et al., 2009).
Terminal or Perisynaptic Schwann cells (PSCs) are found at axon terminals at neuromuscular junctions. They express a variety of molecules, including S100, N-CAM, L1 and myelin-associated protein P0, as well as neuregulin (NRG1/2), and their receptors ErbB2/3. The nerve-derived NRG-1 factor is required for the maintenance and development of neuromuscular junctions. NRG-1 and NRG-2 derived from PSCs, together with NRG-1 derived from the nerve terminal, may play a role in regulating the synthesis of nicotinic acetylcholine receptors (AChRs) in postsynaptic muscle fibers. Among the PSCs-derived molecules, transforming growth factor b, TGFb, enhances synaptogenesis via upregulating the expression of neuronal agrin during development (Figure3). After denervation, the expression of several molecules are upregulated in PSCs after denervation, including GFAP, GAP-43, p75, nestin, and Semaphorin (Sema) 3A (Darabid et al., 2014; Feng and Ko, 2008)

2.5 Nerve Injury and regeneration

Peripheral nerve injuries are a feature of numerous neuromuscular pathologies such as Amyotrophic Lateral Sclerosis (ALS) or a consequence of trauma and, in both cases, impair the patients' quality of life.
There are different classification systems to describe all the many variations of nerve injury. In 1943, Seddon was the first to classify nerve injuries into three categories based on the presence of demyelination and the extent of damage to the axons and the connective tissues of the nerve (Seddon, 1943). In this classification, neurapraxia is the mildest form of injury, where the axon remains intact, but there is myelin damage, causing an asynchronous conduction to conduction block, and leading to muscle weakness. There is a temporary loss of function which is reversible. Neurapraxia typically occurs due to mild compression or in inflammatory neuropathies. The second category is axonotmesis, which involves direct damage to the axons in addition to focal

demyelination while maintaining continuity of the nerves' connective tissues. This type of nerve injury causes paralysis of the motor, sensory and autonomic nerve system, and is mainly seen in crush injury. If the force creating the nerve damage is removed in a timely fashion, the axon may regenerate, leading to the recovery of sensory and motor function in about 3 weeks (Grönholdt-Klein et al., 2019).

The most severe form of injury is called neurotmesis, which is a full transection of the axons and connective tissue layers. The axons lose their continuity and there is a complete loss of sensory and function. Separation of the proximal and distal stumps impedes reinnervation and often leads to the formation of a neuroma.

In the following years, different classifications have been described in the literature, for instance, Sunderland's classification where the distinction was based on the extent of damage in the connective tissues or Thomas and Holdroff's classification based on either non-degenerative or degenerative nerves (Table1).

Following denervation, reinnervation can occur in three ways depending on the type of damage: 1) axon remyelination 2) through collateral branching of intact axons or 3) by regeneration of the injured axon. In neurapraxia, repair mechanisms can rapidly restore nerve conduction by axon remyelination. In the collateral branching of intact axons, the PSCs of denervated NMJs extend processes that guide generating axons from intact NMJs to the vacant synaptic sites (Griffin and Thompson, 2008; Kang et al., 2003, 2014; Magill et al., 2007a).

Seddon	Sunderland	Pathophysiology
Neuropraxia (compression)	Type1	Local myelin damage with the nerve still intact.
Axonotmesis (crush)	Type 2	The continuity of axon is lost. The endoneurium, perineurium, and epineurium remain intact. Loss of continuity of axon with Wallerian degeneration due to disruption of axoplasmic flow.
	Type3	Type3 with endoneurial injury.
	Type4	Type4 with endoneurial and perinuril injury but an intact epineurium.
Neurotmesis (transection)	Type5	Complete physiologic disruption of the entire nerve trunk.

Table 1 Types of nerve damage

Furthermore, the deficiency in PSC bridge formation impairs the efficiency of nerve reinnervation as well as the functional recovery of muscles, as demonstrated in aging muscles and *mdx* mice - murine model of Duchenne Muscular Dystrophy (Kang et al., 2014; Personius and Sawyer, 2005). In injuries affecting axons, the nerve undergoes three main processes: Wallerian degeneration, axonal regeneration, and muscle reinnervation (Menorca et al., 2013). Wallerian degeneration is a clearing process of the distal stump. During this process, Schwann cells (SCs) and macrophages cooperate to remove debris, specifically myelin and damaged axons, from the distal injury site: Schwann cells clear debris through phagocytosis and by recruiting macrophages through the segregation of the monocyte chemoattractant protein-1 (MCP), while macrophages produce factors that promote Schwann cell proliferation. Upon loss of axonal contact, myelinating SCs dedifferentiate and acquire the phenotype of pre/non-myelinating SCs by expressing of p75 low- affinity nerve growth factor receptors

(NGF-R), glial fibrillary acidic protein (GFAP) glial maturation factor-b, the cell adhesion molecule L1 and neural cell adhesion molecule (N-CAM).
The dedifferentiated SCs proliferate and form an endoneurial tube, which provides a path for the regenerating axon to regrow. At the distal tip of the proximal bud, a growth cone is formed. It has been found that calcium plays a role in the proximal stump to promote growth cone formation (Geraldo and Gordon-Weeks, 2009; Stoll and Müller, 2006). SCs produce neurotrophic factors, to promote cone growth. When SCs are re-contacted by regrowing axons, remyelination, axon enlargements and finally functional re-innervation take place. The axonal outgrowth produces ATP and acetylcholine, which promote a change in the SCs' phenotypes from non-myelinating to myelinating (Figure5) (Stoll et al., 1989).

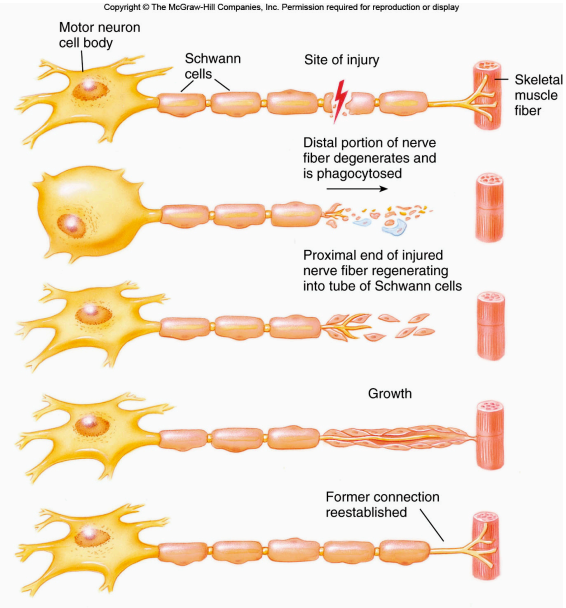

Figure 5 Nerve Regeneration (The McGraw-Hill Companies, Inc.)

2.6 Neurogenic Muscle Atrophy

Neurogenic muscle atrophy is a hallmark of several degenerative processes involved in different pathologies (Bouchè et al., 2018).
During neurogenic muscle atrophy, the interruption of transmission of neurogenic signals to muscle, caused by the loss of neuromuscular junction (NMJ) integrity, activates protein breakdown and reduces protein synthesis, leading to the loss of muscle mass and contractile activity (Bonaldo and Sandri, 2013).
Neurogenic muscle atrophy activates specific signaling pathways and transcriptional programs. For instance, among the upregulated genes, several belong to the protein degradation systems, the ubiquitin-proteasome (UPS) and the autophagy-lysosome. Indeed, the genes induced most strongly were found to encode two muscle-specific E3 ubiquitin ligases, atrogin-1 (also known as MAFbx) and MuRF1, leading to proteasomal degradation of structural muscle proteins (Bodine, 2001; Ehmsen and Höke, 2020; Gomes et al., 2001; Sandri et al., 2004). Overexpression of MAFbx in skeletal myotubes leads to atrophy, whereas knockdown of MAFbx or MuRF1 in mice leads to a significant resistance to skeletal muscle denervation atrophy (Bodine, 2001). Both these ligases were regulated by different pathways, such as the phosphoinositide 3-phosphate (PI3K)-AKT-mTOR signaling pathway (Bodine et al., 2001; Glass, 2005).
Despite the discovery of signaling pathways that control muscle mass, the transcriptional network that orchestrates the expression of genes leading to neurogenic muscle atrophy remains largely unknown. Available evidence suggests that the effect on myofibers caused by neuron loss involves neighboring resident cells. For instance, our group have recently shown that denervation triggers dynamic alterations in the number, gene expression profile and functional interactions between the interstitial cells, Fibro Adipogenic Progenitors (FAPs), and myofibers, in the absence of concomitant infiltration of macrophages and activation of MuSCs. Persistent activation of STAT3 signaling and secretion of IL6 from

FAPs of denervated muscles are necessary and sufficient to promote muscle atrophy (Madaro et al., 2018a).
The role of MuSCs in the atrophic process remains controversial (Pallafacchina et al., 2013). Our group did not observe a significant change in MuSCs content in atrophying mouse muscle at 3, 7, or 15 days post-denervation (Madaro et al., 2018a). Instead, previous studies display a modest albeit significant increase in MuSCs number 6 weeks after denervation. Furthermore, they show that MuSCs depletion leads to deficits in skeletal muscle reinnervation, reductions in post-synaptic morphology and loss of post-synaptic myonuclei (Liu et al., 2015a, 2017). Exploring the involvement of MuSCs and the other muscle resident cells, and their crosstalk, in this context could pave the way towards the development of new possible therapeutic approaches to counteract the neurogenic muscle atrophy.

2.7 Amyotrophic Lateral Sclerosis

Amyotrophic Lateral Sclerosis (ALS) is a fatal neurodegenerative disease, characterized by the degeneration of upper and lower motor neurons, which leads to a deterioration of neuromuscular function, progressively causing muscle weakness, fasciculation, muscle atrophy, speech and swallowing disabilities, progressive paralysis, and ultimately death due to respiratory failure. ALS can be sporadic (90–95%) - without any obvious genetic component - and familial (5–10%), usually with an autosomal-dominant pattern of inheritance (Rowland and Shneider, 2001). Among the genetic mutation, Superoxide dismutase 1 (SOD1) is mutated in the majority of the case of familial ALS (fALS) and also contributes to some of the sporadic ALS cases (sALS). Other genes involved in ALS development have been described including TAR DNA-binding protein 43 (TDP43) or the Fused-in-sarcoma (FUS) gene – that encode for a protein implicated in RNA splicing (Liscic and Breljak, 2011; Mirra et al., 2017), as well as the more recently identified alterations of the frequency of a hexanucleotide repeat expansion in

the non-coding region of the C9ORF72 seen in most of the fALS (Majounie et al., 2012).
Notably, sporadic and familial ALS have similar pathological hallmarks. Multiple pathogenic mechanisms have been proposed to contribute to motor neuron degeneration, including excitotoxicity, oxidative stress, aberrant protein aggregation, defective axonal transport, mitochondrial dysfunction and altered RNA metabolism. However, the precise nature of the selective loss of motor neurons remains obscure.
The progression of ALS is usually fast and patients' death typically occurs within 1-5 years of diagnosis (Therrien et al., 2016). Despite extraordinary efforts over the last two decades, no biomarkers or effective therapeutic approaches have been identified. In order to prolong their lives, patients undergo tracheostomy-delivered assisted ventilation. Ultimately patients develop motor paralysis known as a 'totally locked-in state', where the paralysis of all voluntary muscles and oculomotor impairment takes place. Currently, Riluzole, a chemical derivative of 2-aminobeanzothiazole, is the pharmacological treatment approved for ALS by the FDA and EMA. However, the mechanisms of action of Riluzole are not really understood and questions persist about its clinical utility because of its high cost and modest efficacy (prolongs median survival by about two to three months) (Mathis et al., 2017; Miller et al., 2007). Recently, Edravone - a member of 2-pyrazolin-one family - has been approved by FDA for the treatment of ALS. This molecule works in the central nervous system as a potent scavenger of oxygen radicals. Clinical trials revealed that the decline in motor, speech, swallowing and respiratory function was significantly less severe in patients treated with Edaravone (Traynor, 2017). In spite of this, there is still no curative treatment for ALS.
ALS shows large phenotypic variability in both sporadic or familial forms and many studies have pointed out the pathological role of different cell types – other than neurons. Moreover, most of ALS cases are believed to be caused by the effect of environmental factors such as exposure to virus, fertilizers, heavy metals, diet and others (Yu and Pamphlett, 2017).

2.8 ALS and skeletal muscle

Muscle denervation by progressive loss of the neuromuscular junction (NMJ) is thought to play a crucial role in ALS. However, the molecular pathogenesis of ALS remains elusive and the triggering events leading to specific motor neuron degeneration are unclear.

The primary role of skeletal muscle in ALS progression is still controversial (Loeffler et al., 2016). Several lines of evidence support the hypothesis supporting that muscle damage can lead to the onset of ALS pathology through a so-called retrograde dying-back of the motor neurons. Fischer's group demonstrated that before any loss of motor neurons, there is a severe loss of ventral root motor axons and a significant denervation at corresponding neuromuscular junctions in $SOD1^{G93A}$ mutant mice, a widely used transgenic ALS mouse model, and in ALS human biopsies (Fischer et al., 2004). Kraft's group provided evidence that, in $SOD1^{G93A}$ mutant mice expressing an antioxidant response element (ARE), the activation of an antioxidant response occurs in the distal muscles and appears to progress in a retrograde fashion along the motor neurons (Kraft et al., 2007). Based on magnetic resonance imaging, the muscle volume in $SOD1^{G93A}$ mice was significantly reduced from as early as week 8 of life, 4 weeks prior to clinical onset, while neurodegeneration occurs later, after clinical onset, at weeks 10-18 (Marcuzzo et al., 2011).

Other studies promote the hypothesis that skeletal muscle directly influences the NMJ stability and nerve degeneration (Dobrowolny et al., 2008; Wong and Martin, 2010). Indeed, it has been shown that the muscle-specific expression of the mutated SOD1 in mice leads to muscle atrophy and skeletal muscle functional impairment (Dobrowolny et al., 2008). Finally, it has been shown that preserving the NMJ is sufficient to delay neuron degeneration, improving motor function and delaying the onset of the disease in a mouse model of ALS (Pérez-García and Burden, 2012).

In this context, increasing the knowledge about the role of nerve-muscle crosstalk can help to solve some of these caveats.

2.9 ALS mouse model: $SOD1^{G93A}$

In 1993, the first causative gene for ALS was discovered, encoding the enzyme Cu/Zn superoxide dismutase 1 (SOD1). More than 150 mutations of the SOD1 have been identified in fALS (Deng et al., 1993; Gurney et al., 1994; Rosen et al., 1993). Transgenic mice carrying the human SOD1 mutations develop a phenotype similar to ALS patients, making them useful as models to understand the pathogenesis of disease and to test new therapies. In the SOD^{G93A} mouse model, the mutation is a substitution of glycine to alanine at position 93 - a change that has little effect on enzyme activity. The neurotoxicity associated with mutant SOD1 is not well understood. It is possible that the neurotoxicity deriving from the presence of mutated SOD may be the result of a detrimental new function acquired by the mutated enzyme: mutant SOD1, indeed, is prone to form aggregates that may lead to neuron cytotoxicity. In SOD^{G93A} mouse model, the clinical disease onset starts at 91 +/- 14 days of age with fine shaking of the limbs, followed by paralysis and death by 136 +/- 7 days of age (Chiu et al., 1995).

3. AIMS

The main objective of my Ph.D. project is to dissect the molecular and cellular mechanisms that control neurogenic muscle atrophy with particular attention on the role of muscle resident cells.
Our recent study showed that during both traumatic denervation and in a mouse model of Amyotrophic Lateral Sclerosis (ALS), Fibro Adipogenic Progenitors (FAPs) progressively accumulate in the skeletal muscle. Moreover, a specific gene expression program characterized by the activation of the IL-6/STAT3 axis was observed in FAPs following nerve injury. Inhibition of this pathway was sufficient to reduce muscle atrophy and fibrotic deposition in both acute denervation and ALS. Altogether, these observations reveal a novel biological activity of FAPs in denervated muscles, characterised by the generation of both pro-atrophic and pro-fibrotic signals (Madaro et al., 2018b). Previous studies have shown that MuSCs depletion impairs skeletal muscle reinnervation (Liu et al., 2015b, 2017). However, using the denervated mouse model, we did not observe a significant increase of satellite cell (MuSC) number; suggesting that the role of MuSCs in these processes is unclear. We therefore decided to examine the transcriptional profiles of Itg7a-expressing MuSCs isolated from limb muscles of mice either unperturbed or exposed to nerve injury by focusing on the following specific aims:
-Aim1: Characterization of the Itga7+ cell transcriptome in both bulk and single cells isolated from limb muscle of mice 3 days following nerve injury in order to identify the cellular and molecular players that might contribute to nerve repair. For this purpose, we performed both RNAseq and Single cell RNA-seq analysis on Itga7+/Sca1-/Ln- cells. To validate the results of these analyses we performed RT-qPCR and Immunofluorescence experiments.
-Aim2: Assess the activation of a neurotrophic program in the Itga7+ cells, to formally determine whether this activation occurs in cells derived from the satellite cells pool or other Itga7 expressing cells. For this purpose, we used 3 months old tamoxifen-treated the $PAX7^{CreER}$;$tdTomato^{f/f}$ mice, in order to trace SCs fate during

denervation. Indeed, Tamoxifen administration results in the labeling of Pax7+ MuSCs with Tomato fluorescent protein (Liu et al., 2015b; Nishijo et al., 2009). After denervation, cells that express Pax7 can be isolated before denervation to perform molecular analysis.

-Aims3: Investigate the biological link between NMJ stability and the activation of a neurotrophic program after denervation. To this end, we studied the crush injury model that allows us to assess the effect of reinnervation, at 30 days post nerve injury.

-Aims4: Examine the neurotrophic program activation following other conditions where the NMJ is impaired, due to traumatic damage (spinal cord injury-SCI), or pathological conditions (ALS).

-Aim5: Functional studies of these Itga7+ cells isolated from limb muscle of mice 3 days following denervation. To study the ability of these Itga7+ cells to activate a neurotrophic program, we performed co-culture experiments with neuronal cells, using trans-well inserts, which allows the study of the indirect interaction (soluble factors).

Unravelling the molecular and cellular mechanisms that govern the crosstalk between muscle resident cells and motoneurons is critical for our understanding of the role of these cells during neurogenic muscle atrophy, and for the identification of novel molecular mediators as potential targets to promote muscle reinnervation and counteract the effects of denervation.

4. RESULTS

4.1 Activation of a neurotrophic signaling pathway in Itga7+Sca1-Ln- cells

The contribution of Itga7-expressing MuSCs to the maintenance of NMJ integrity and regeneration upon nerve injury was previously reported by Liu et al 2015 and Liu et al. 2017 (Liu et al., 2015a, 2017). However, the precise molecular mechanisms and the roles of these Itga7-expressing MuSCs remain largely unknown.

To this end, we performed RNAseq analysis on Itga7+/Sca1-/Ln- cells (from now on, referred to as Itga7+ cells) isolated by FACS from limb muscles of 3-month-old mice, at 3 days after denervation by sciatic nerve severing, and compared to Itga7 cells isolated from control mice. Heatmap comparison revealed extensive alterations of the transcriptional profile in Itga7+ cells isolated post-nerve injury, compared to unperturbed controls, with a clear bias toward the up-regulation of genes which accounted for the vast majority of the differentially expressed genes (Figure 6a).

Notably, most of the upregulated genes were those associated with neuronal growth and repair pathways, including Nerve Growth Factor Receptor (Ngfr), Sonic Hedgehog (Shh) Tenascin-C (Tnc), Neuronal Cell Adhesion Molecule (NRCAM), Glial Cell-Derived Neurotrophic Factor (Gdnf), and the glial lineage-specific transcription factors Oligodendrocyte lineage genes (Olig1) (Figure 6a). Other genes of alternative mesenchymal lineages, but recently implicated in neurogenesis (e.g. Runx2) (Tiwari et al., 2018) were also found upregulated in Itga7+ cells isolated following nerve injury. Moreover, gene ontology analyses of RNAseq data predicted the activation of “nervous system development” and “axon guidance” among the main activated pathways (Figure 6b).

The upregulation of neurotrophic genes in Itga7+ cells after denervation suggests that this population includes cell types endowed with potential nerve repair activities. Thus, to identify this population, we sought to determine whether the activation of the neurotrophic gene program also occurred in Itga7+ cells isolated

from muscles subjected to sciatic nerve crush - a reversible lesion that is typically followed by repair and restoration of NMJ integrity (Magill et al., 2007b). Indeed, the upregulation of neurotrophic genes was also detected by qPCR analysis in Itga7+ cells following sciatic nerve crush (Figure 6c). Interestingly, activation of the same genes was also observed in cells isolated using the Satellite Cells isolation kit (Miltenyi Biotec) magnetic strategy that is based on lineage marker exclusion of Itga7-negative muscle-resident cells (Figure 6d).

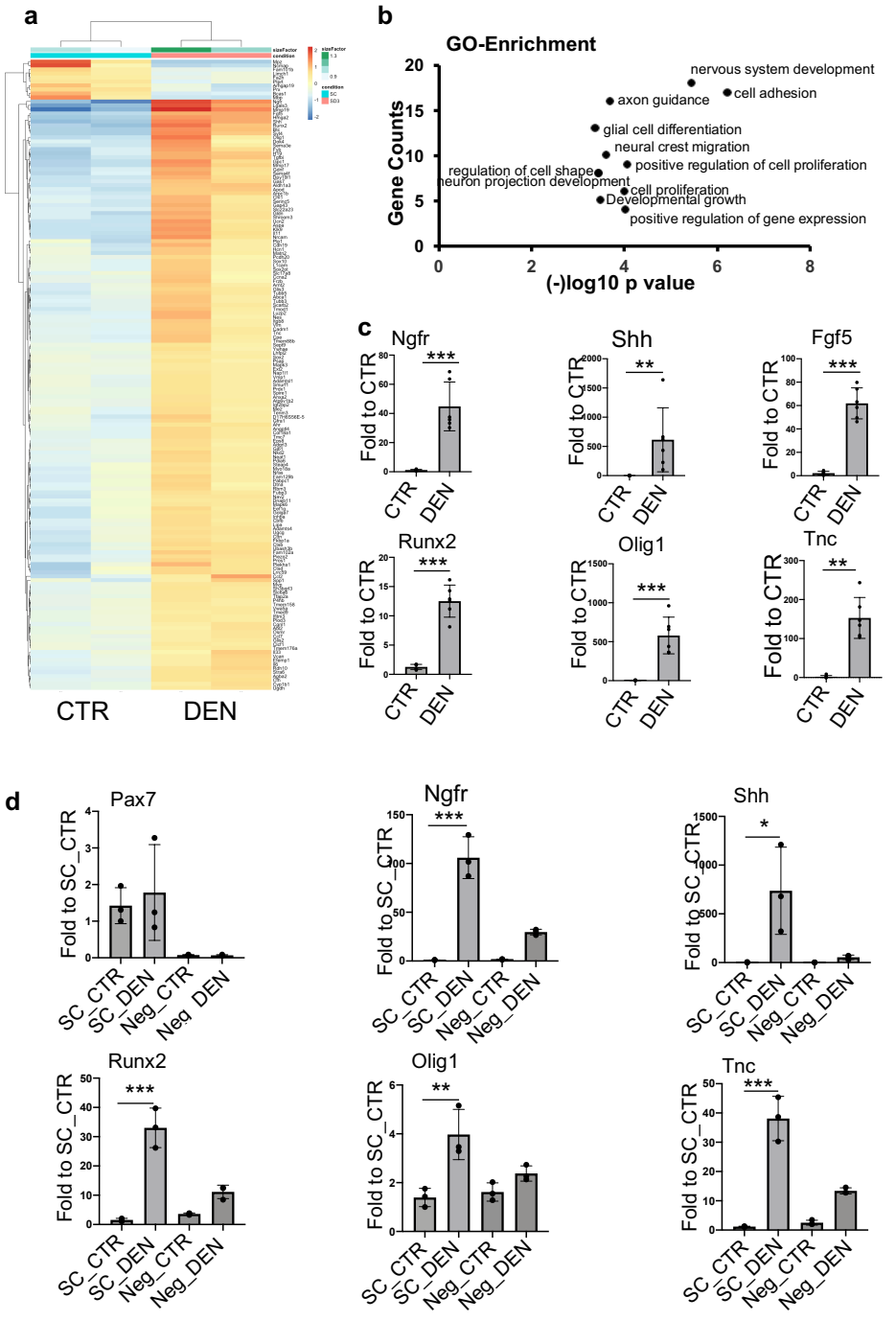
a
CTR
DEN
b
GO-Enrichment
Gene Counts
(-)log10 p value
nervous system development
cell adhesion
axon guidance
glial cell differentiation
neural crest migration
positive regulation of cell proliferation
regulation of cell shape
neuron projection development
cell proliferation
Developmental growth
positive regulation of gene expression
c
Ngfr
Shh
Fgf5
Runx2
Olig1
Tnc
Fold to CTR
CTR
DEN
d
Pax7
Ngfr
Shh
Runx2
Olig1
Tnc
Fold to SC_CTR
SC_CTR
SC_DEN
Neg_CTR
Neg_DEN

Figure 6 Activation of neurotrophic signaling pathway in Itga7+Sca1-Ln- cells. **a)** Heatmap representation of genes significantly deregulated - p adj<0.001 - in Itga7+Sca1-Ln- freshly isolated cells derived from denervated (cut) muscle at 3-days post nerve lesion (n=2). **b)** GO-Enrichment in Biological Function (BF) of genes significantly deregulated - p adj<0.001 - in Itga7+Sca1-Ln- cells derived from at 3 days denervated muscle. **c)** qPCR analysis for the expression of Ngfr, Shh, Fgf5, Runx2, Olig1 and Tnc in freshly isolated Itga7+Sca1-Ln- cells derived from control and 3 days reversible denervated (crush) muscle. Gapdh was used as housekeeping gene [n≥5, Values represent mean ± s.d. **P < 0.01 and ***P < 0.001; by student t-test (Ngfr, Fgf5, Olig1, Runx2, Shh) and Mann-Whitney test (Tnc)]. **d)** qPCR analysis for the expression of Pax7, Ngfr, Shh, Runx2, Olig1 and Tnc in freshly isolated cells from control and denervated muscle isolated with *Satellite Cells isolation kit – Miltenyi Biotec* (SC) or the negative fraction (Neg). Gapdh was used as housekeeping gene (n=3, Values represent mean ± s.d. *P < 0.05, **P < 0.01 and ***P < 0.001; by One Way Anova test).

4.2 Nerve injury activates a neurotrophic program in Itga7+ Pax7- non-satellite cells

Given the recent studies showing that Itga7-expressing cells include cell subsets divergent in developmental origin from the true MuSCs (Giordani et al., 2019), we utilized the PAX7^{CreER};tdTomato$^{f/f}$ mouse model, which allows MuSCs lineage tracing (Tierney et al., 2016), in order to unequivocally determine whether the activation of the neurotrophic gene program occurs in MuSCs or the non-MuSC cell fraction among the Itga7+ cells. Seven days after tamoxifen treatment, 3-month-old mice were subjected to nerve injury and analyzed 3 days later (Figure 7a). In this mouse model, tamoxifen treatment leads to the permanent expression of tomato fluorescent protein in Pax7+ MuSCs (Figure 7b). As expected, Itga7+Tomato+ cells isolated from limb muscles of mice either unperturbed or subjected to sciatic nerve crush expressed high levels of the MuSC-identity gene Pax7 and Vcam1 (Figure 7c), whereas the Itga7+Tomato- cell population did not express these markers. However, upon denervation, only the Itga7+Tomato- fraction expressed Ngfr, Shh, Tnc, Nrcam, Gdnf and Plp1, indicating the induction of a neurotrophic signaling pathway in the Pax7-negative fraction of Itga7+ cells (Figure 7c). These observations also indicate that between cells isolated with the Satellite Cells isolation kit (Miltenyi Biotec) a Pax7 negative population co-segregate with the myogenic fraction.
Overall, these findings show transcriptional activation of a neurotrophic program in the non-myogenic fraction of Itga7+ cells and suggest their potential involvement in the functional cross-talk between muscle resident cells and NMJ in response to nerve injury.

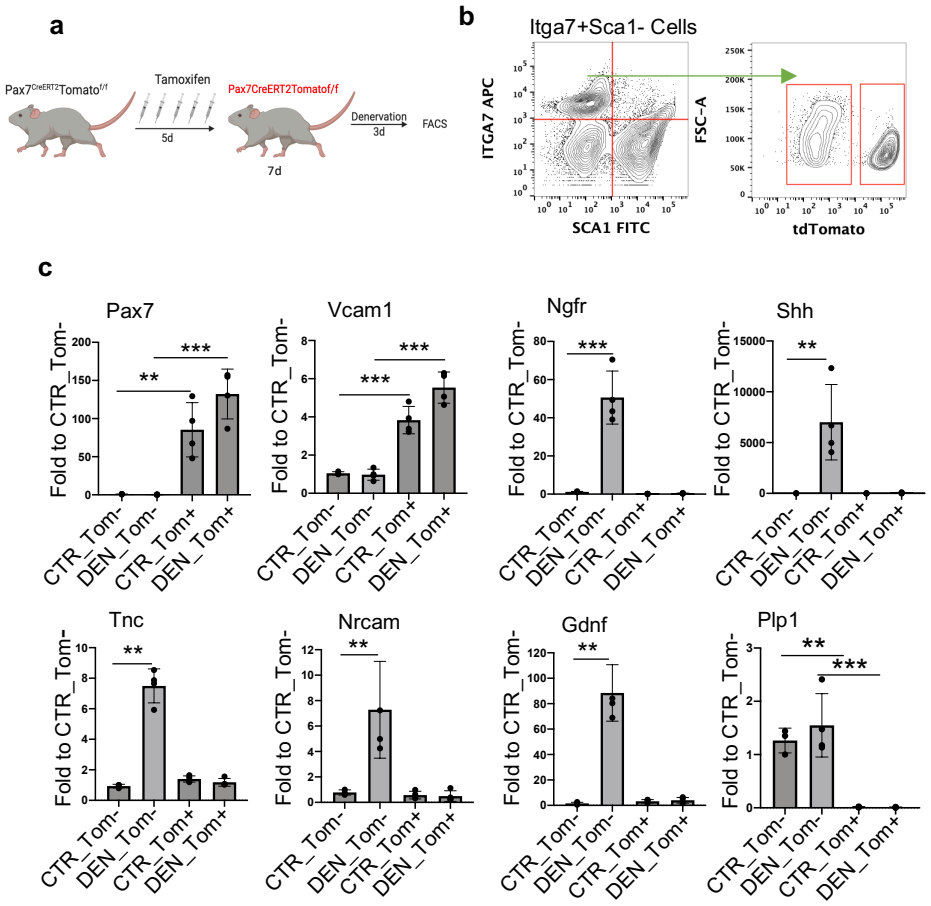

Figure 7 Nerve injury activates a neurotrophic program in Itga7+ Pax7- non-satellite cells. **a)** Working model of tamoxifen induced in-vivo treatment. **b)** FACS plot profile of Itga7+ cells freshly isolated from tamoxifen treated PAX7.Cre_tdTomato mice. **c)** qPCR analysis for the expression of Pax7, Vcam1, Ngfr, Shh Tnc, Nrcam, Gdnf and Plp1, in freshly isolated Tomato+ and Tomato- cells derived from control and 3 days denervated muscle of tamoxifen treated PAX7.Cre_tdTomato mice. Gapdh was used as housekeeping gene (n=4, Values represent mean ± s.d. **P < 0.01 and ***P < 0.001; by One Way Anova test.).

4.3 scRNA-seq reveals heterogeneity within the Itga7+ muscle resident cells

Recently, the heterogeneous composition of muscle resident mononuclear cells has been dissected using high resolution cartography by scRNA-seq. This strategy has revealed the identity of a new MuSCs-independent myogenic population among the Itga7+ cells, referred to as Smooth Muscle Mesenchymal Cells (SMMCs)(Giordani et al., 2019). To further determine whether the activation of the neurotrophic program upon nerve injury occurred in SMMC or other sub-populations within Itga7+ cells, we performed single-cell RNA-seq (scRNA-seq) transcriptome profiling in Itga7+ cells isolated from limb muscles of mice 3 days following sciatic nerve crush or control mice. By using the 10x Genomics' single-cell RNA-seq (scRNA-seq) technology we obtained a total of 3949 cells analyzed. Clustering analysis identified 11 different groups (Data not shown). Based on markers expression we could clearly identify three major populations that were composed of multiple sub-clusters (Figure8a-b). In particular, we detected MuSCs, as Pax7+, Myf5+ and Vcam1+ expressing cells, smooth muscle mesenchymal cells (SMMCs), as Myh11+ expressing cells and glial cells as Plp1 and Mpz expressing cells (Figure 8a).

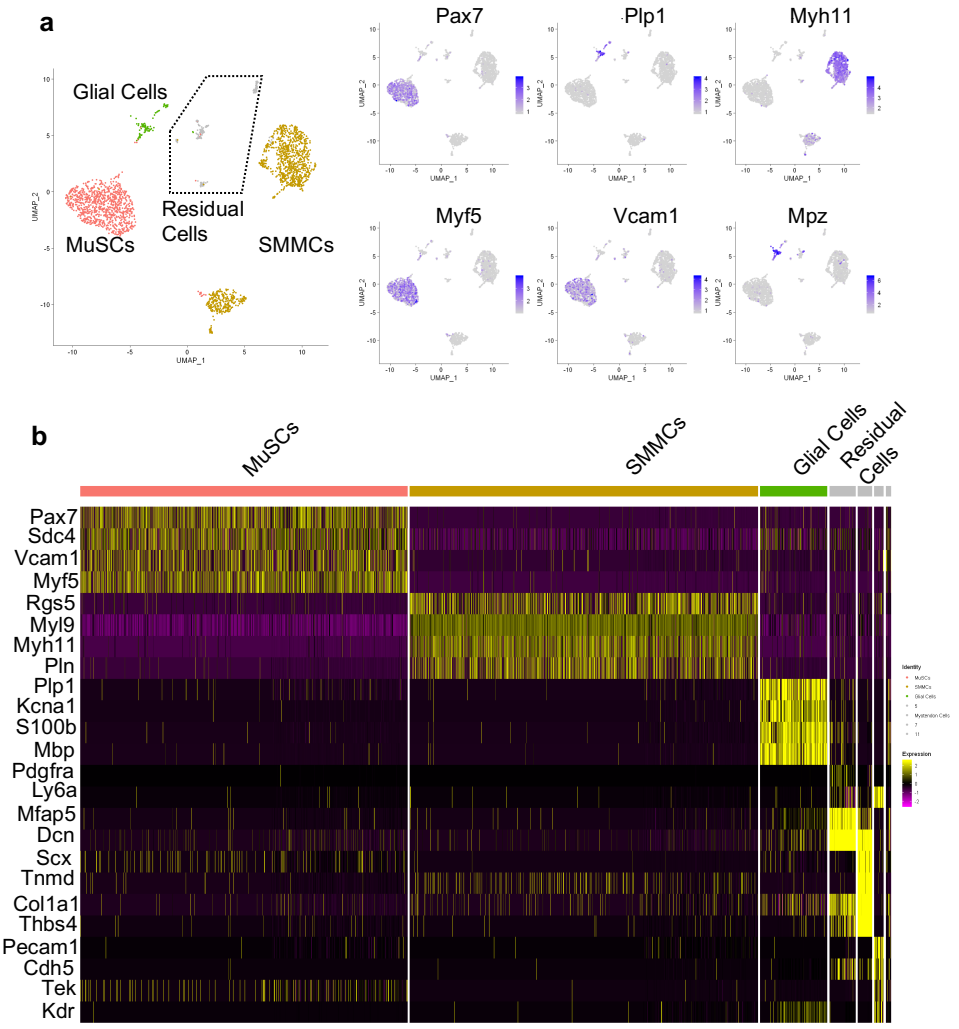

Figure 8 Itga7+ cells heterogenicity resolution by scRNA-seq analysis. **a)** Distribution of Pax7, Plp1, Myh11, Myf5, Vcam1 and Mpz transcripts in Uniform Manifold Approximation and Projection (UMAP)-derived clusters of single cells (Single Cells RNA-seq) of Itga7+Sca1-Ln- isolated cells from control muscle. **b)** RNA expression heatmap for the given cell populations (column) and genes (row), sorted by clusters. The canonical markers used to identify each cluster are plotted (or the most variable genes per cluster in cases where markers were not already present in the literature).

4.4 Plp1+ glial cells are the major Itga7+ population responsive to denervation

We focused our analysis on the three major cell types identified by scRNAseq analysis among the Itga7+ cells isolated following nerve injury – i.e. MuSCs, SMMCs and glial cells. We observed a similar distribution of MuSCs and SMMCs in both healthy and denervated muscle (Figure 9a). By contrast, we observed a specific increase in Plp1+ cells in response to nerve injury. Furthermore, we noted extensive alterations in gene expression in Plp1+ cells following nerve injury, compared to control muscle, while only a few genes were significantly altered in MuSCs and SMMCs (Figure 9b). Single cell RNAseq analysis revealed that Plp1+ glial cells are characterized by a neurotrophic signature (Figure9b-d), with most of the upregulated genes coinciding with those identified in the bulk Itga7+ cells shown in Figure 6 – i.e. Ngfr, Tnc, Gdnf, Runx2 and other genes strictly related to nerve development (Figure 9c).
To validate if the activation of Plp1+ cells is associated with their proliferation, we denervated mice by nerve crush injury, and at 12h before harvest, we administered an intraperitoneal injection of EdU. EdU incorporation analysis revealed a significant proportion of proliferating Plp1+ cells at 3 days following sciatic nerve crush. (Figure 9e).

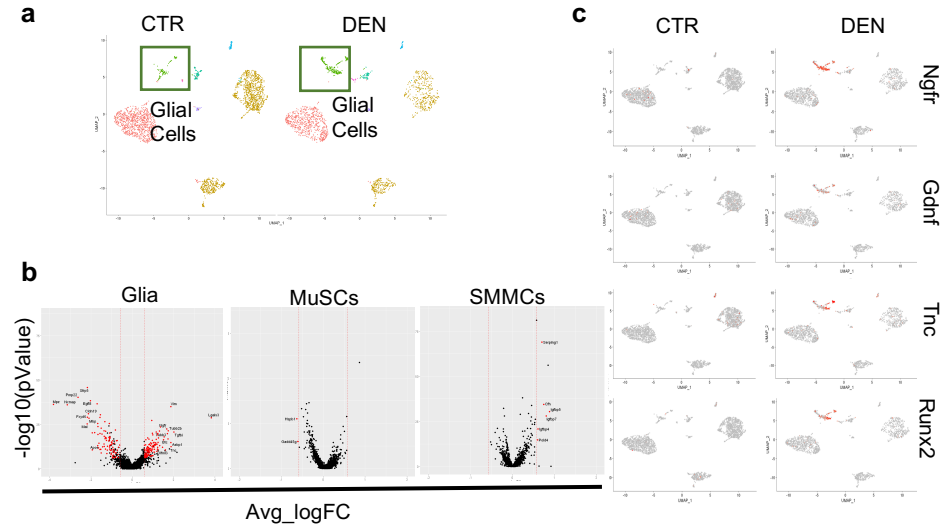
a
CTR
DEN
Glial Cells
Glial Cells
b
Glia
MuSCs
SMMCs
-log10(pValue)
Avg_logFC
c
CTR
DEN
Ngfr
Gdnf
Tnc
Runx2

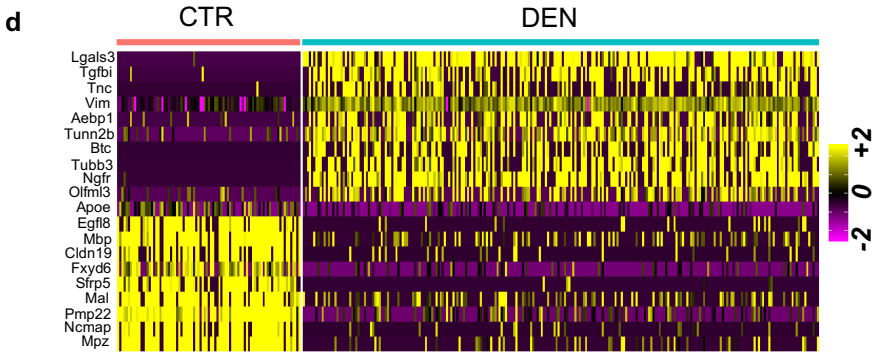
d
CTR
DEN
Lgals3
Tgfbi
Tnc
Vim
Aebp1
Tunn2b
Btc
Tubb3
Ngfr
Olfml3
Apoe
Egfl8
Mbp
Cldn19
Fxyd6
Sfrp5
Mal
Pmp22
Ncmap
Mpz
+2
0
-2

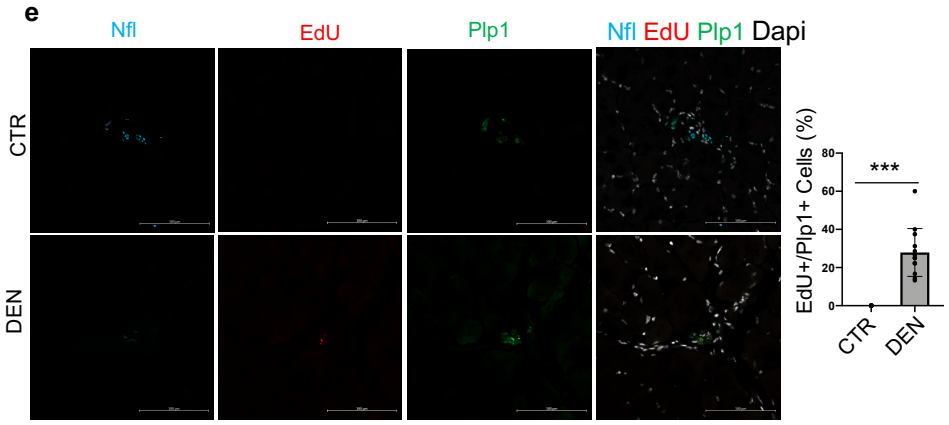
e
Nfl
EdU
Plp1
Nfl EdU Plp1 Dapi
CTR
DEN
EdU+/Plp1+ Cells (%)
***
CTR
DEN

Figure 9 Activation of neurotrophic signalling pathway in muscle glial cells upon denervation. **a)** Distribution in Uniform Manifold Approximation and Projection (UMAP)-derived clusters of single cells (Single Cells RNA-seq) of Itga7+Sca1-Ln- isolated cells from control (CTR-left) and 3-days denervated muscle (DEN-right). **b)** Volcano plots for differentially expressed transcripts represents the logarithm of average fold change (Avg_logFC) on x-axis and log10 of the q-value of each transcripts on y-axis; The significative changes induced by denervation was shown for Glia, MuSCs and SMMCs. **c)** Distribution of Ngfr, Gdnf, Tnc and Runx2 transcripts in Uniform Manifold Approximation and Projection (UMAP)-derived clusters of single cells (Single Cells RNA-seq) of Itga7+Sca1-Ln- isolated cells from control (left) and denervated (right) muscle. **d)** RNA expression heatmap for Plp1 cell populations isolated from control and denervated muscle (row) and genes (column), sorted by clusters. **e)** Representative immunofluorescence analysis of TA muscle cryosection derived from control and denervated muscle, stained for Neurofilament-L (Nfl, Cyan), EdU (red) and Plp1 (green). Nuclei were counterstained with dapi. Scale bar = 100μm. (right) Graph representing the percentage of Plp1+EdU+ cells in cryosection of control and denervated muscle. (n=9 slide of 3 different animals. ***$P < 0.001$; by student t-test).

4.5 Ngfr+ cells are activated glial cells in the muscle upon denervation

Among the upregulated genes in glial cells in muscle upon denervation, we used Ngfr to identify these cells, since it was found to be specifically expressed in glial-cells, and no other muscle resident cells, in response to nerve injury by an independent scRNAseq analysis post-denervation (PLP unpublished data). It is interesting to note that Hicks et al. have previously shown that Ngfr is transiently expressed in human MuSc progenitors during the generation of hiPSC-derived MuSCs (Hicks et al., 2018). Our data indicate that Ngfr expression discriminates glial cells from MuSCs within a common pool of Itga7+ cells. Indeed, Ngfr+ cells were only detected among the Itga7+ population in the muscle at 3 days after denervation, while only a negligible number of Ngfr+ cells were present in the control muscle (Figure 10a-c,). There were no significant changes in the number of Ngfr-Itga7+ cells after nerve injury (Figure 10b), thus confirming that the main cell type responding to denervation are the muscle- resident glial cells. We found that in unperturbed muscles Plp1 positive cells are close to the neuron structure stained for Neurofilment (NF-L) that is lost upon nerve injury. However, upon neve injury, Plp1+ /Ngfr+ cells were found in a structure reminiscent of the nerve structure (Figure 10c). Moreover, the induction of neurotrophic genes, including Ngfr but also Plp1, Tnc, Nrcam and Gdnf, was only detected in Ngfr+ but not Ngfr- cells isolated from denervated muscle (Figure 10d). Finally, Ngfr+ cells exert a different phenotype in-vitro compared with Ngfr- population, and unlike Ngfr- cells are not myogenic (Figure 10e-f).

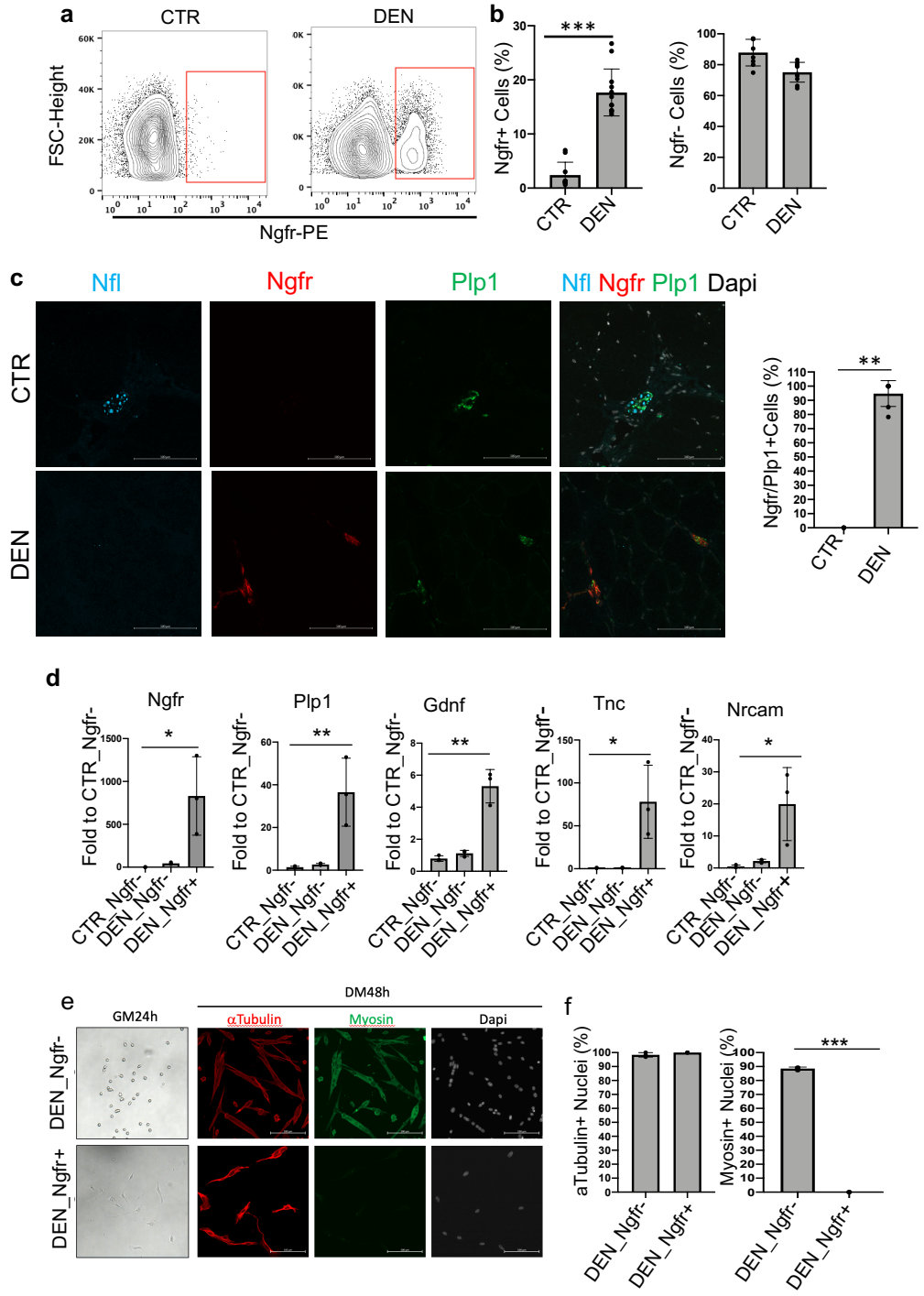
a
CTR
DEN
FSC-Height
Ngfr-PE
b
Ngfr+ Cells (%)
Ngfr- Cells (%)
CTR
DEN
c
Nfl
Ngfr
Plp1
Nfl Ngfr Plp1 Dapi
CTR
DEN
Ngfr/Plp1+Cells (%)
d
Ngfr
Plp1
Gdnf
Tnc
Nrcam
Fold to CTR_Ngfr-
CTR_Ngfr-
DEN_Ngfr-
DEN_Ngfr+
e
GM24h
DM48h
αTubulin
Myosin
Dapi
DEN_Ngfr-
DEN_Ngfr+
f
aTubulin+ Nuclei (%)
Myosin+ Nuclei (%)

Figure 10 Ngfr+ glial cells active a neurotrophic program after denervation. **a)** Representative cytofluorimetric plot of Ngfr+ - gated within the Itga7+Sca1-Ln- population - cells in control (left) and denervated (right) muscle. **b)** Quantification of Ngfr+ (left) and Ngfr- (right) cells was shown in the graphs as a percentage of Itga7+Sca1-Ln- population (n=8 CTR, n=10 DEN, Values represent mean ± s.d. ***P < 0.001; by Mann-Withney test). **c)** Representative immunofluorescence analysis of TA muscle cryosection derived from control (CTR) and denervated (DEN) muscle, stained for Neurofilament-L (Nfl, Cyan), Ngfr (red), Plp1 (green). Nuclei were counterstained with dapi. Scale bar = 100μm. (right) Quantification graph of Ngfr+/Plp1+ cells in control (CTR) and denervated (DEN) muscle (n=7, Values represent mean ± s.d. **P < 0.01; by Mann-Whitney test. **d)** qPCR analysis for the expression of Ngfr, Plp1, Gdnf, Tnc, Nrcam in freshly isolated Ngfr+ or Ngfr- cells derived from control and 3 days denervated muscle. Gapdh was used as housekeeping gene (n=3, Values represent mean ± s.d. *P < 0.05 and **P < 0.01; by One Way Anova test). **e)** In-vitro culture of both Ngfr- and Ngfr+ cells. Phase contrast images of proliferating cells was shown (left panel). Representative immunofluorescence analysis for αTubulin (Red) and Myosin (green) was performed 48h after myogenic differentiation. Nuclei were counterstained with dapi. Scale bar = 100μm. **f)** Quantification of αTubulin and Myosin of both Ngfr- and Ngfr+ cells *in-vitro* culture (n=3, Values represent mean ± s.d. ***P < 0.001; by student t-test).

4.6 Ngfr+ cells in muscular and in nerve tissue activate a different gene expression programs upon denervation

Activated glial cells are known to respond to nerve injury and participate in nerve repair and axon guidance. To exclude the possibility that the presence of activated glial cells within the muscle was simply caused by co-isolation of adjacent tissues (i.e. nerves), we compared the gene expression profile of Ngfr+ cells isolated from nerves or muscles at 3 days after nerve injury (Figure 11a). Transcriptome analysis revealed significant differences between the two populations, which clearly formed two independent clusters with a large subset of differentially regulated genes (Figure 11b-c). Interestingly, among the genes differentially expressed by the two glial cells we found some genes more represented in muscle derived glial cells (i.e. Tnc, Gdnf), while others are more expressed in neuron derived cells (i.e. Shh) (Figure 11d). We focused on Tnc since its ablation is known to delay NMJ recovery in-vivo. Tnc protein unequivocally localized close to bungarotoxin (BTX) NMJ upon denervation (Figure 11e).
These results suggest an involvement of Tnc in the maintenance of NMJ in the absence of innervation.

\

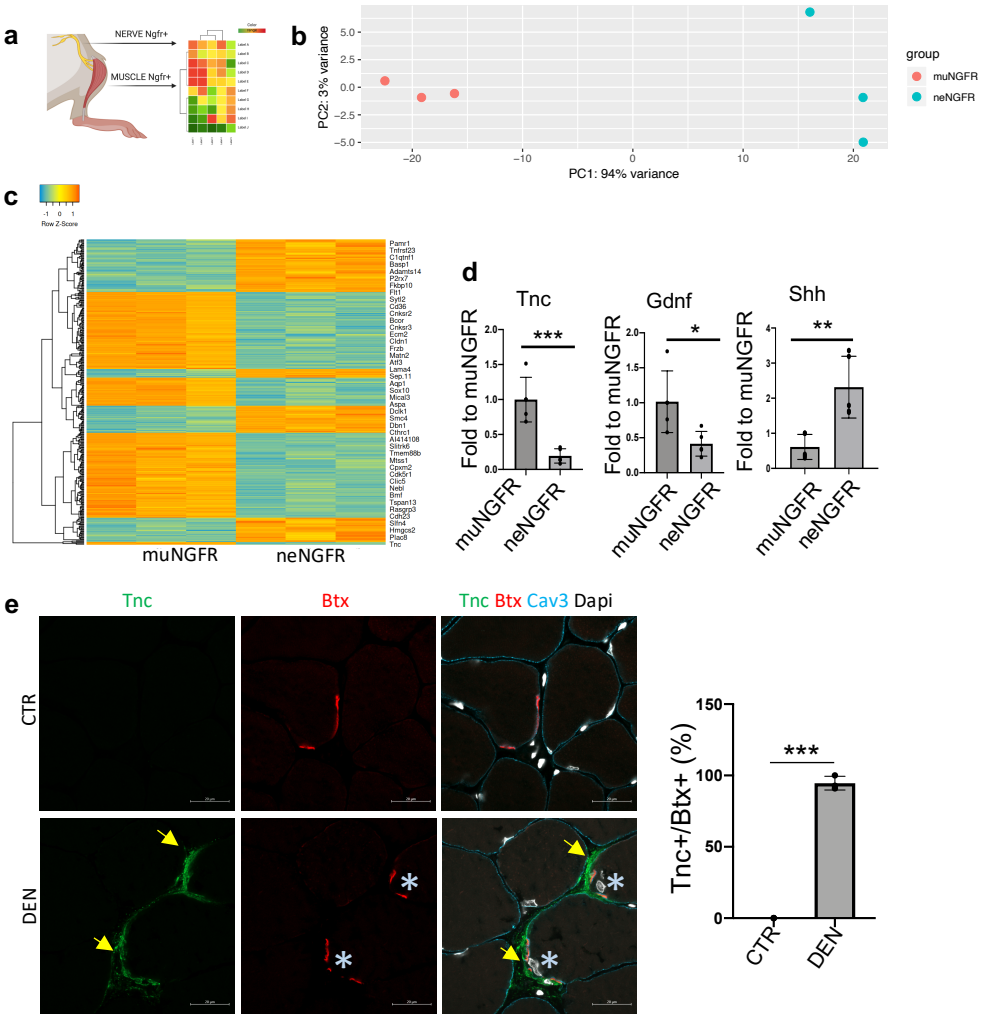

Figure 11 Ngfr+ cells in muscular and in nerve tissue activate a different gene expression programs after denervation. **a)** Experimental setting for RNA-sequencing analysis of Ngfr+ cells derived from denervated muscle and nerve at 3-days post nerve lesion. **b)** Sample distance - represented as Principal component analysis (PCA) - of transcriptome of Ngfr+ cells derived from denervated muscle and nerve at 3-days post nerve lesion (n=3). **c)** Heatmap representation of genes significantly deregulated - p adj<0.001 – in freshly isolated Ngfr+ cells derived from denervated muscle and nerve at 3-days post nerve lesion (n=3). **d)** qPCR analysis for the expression of Tnc, Gdnf and Shh in freshly isolated Ngfr+ cells derived from denervated muscle (muNGFR) and nerve (neNGFR) at 3-days post nerve lesion (n=4, Values represent mean ± s.d. .*P < 0.05, **P < 0.01 and ***P

< 0.001; by student t-test.). **e)** Representative immunofluorescence analysis of TA muscle cryosection derived from control and denervated muscle, stained for Tnc (green), Bungarotoxin (Btx, red) and Caveolin-3 (Cav3, Cyan). Arrows highlight Tnc and asterisk highlight Btx. Nuclei were counterstained with dapi. Scale bar = 20□m. Quantification of the co-localization Bungarotoxin (Btx) and Tnc on the right (n=3, Values represent mean ± s.d. ***P < 0.001; by student t-test).

4.7 The neurotrophic program switches off in Ngrf+ cells upon reinnervation

Crush injury is an acute traumatic compression of the nerve that does not result in a complete transection of the nerve. It is a reversible lesion that is typically followed by repair and restoration of NMJ integrity. The full recovery of sensory and motor function occurs in about 4 weeks (Grönholdt-Klein et al., 2019). For this reason, nerve crush injuries are commonly used to examine peripheral nerve regeneration.

Following crush damage, a reduction of muscle mass and myofibre caliber (during the first 15 days) were typically followed by recovery of muscle weight and myofibre size at 30 days after nerve damage (Figure12a-b-c).

The neuron structure, stained for NF-L, is lost at 3 days after nerve injury, while reinnervation occurs at 30 days after the crush injury (Figure 12d). Moreover, a decline in the number of the Ngfr+ cells and, more importantly, a decrease in the expression of neurotrophic factors were observed after the reinnervation process (Figure 12 e-f).

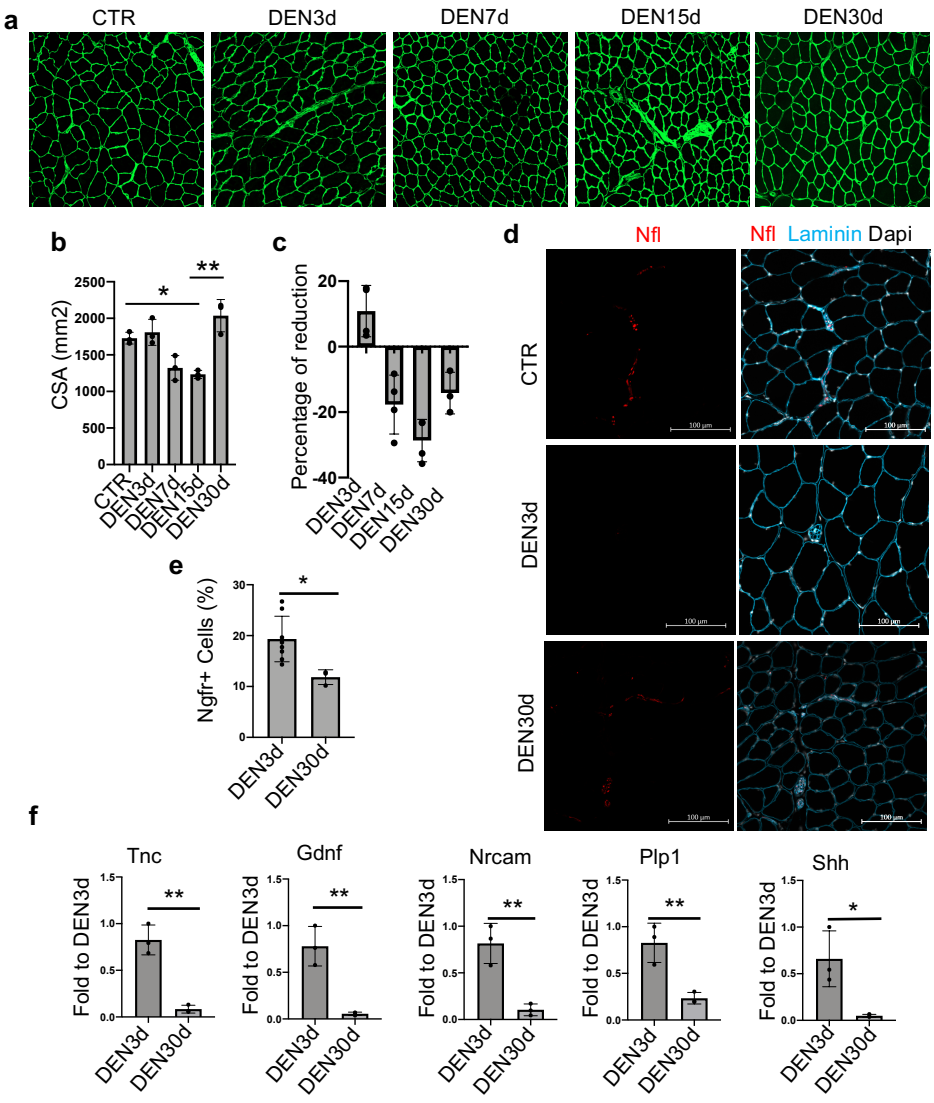

Figure 12 Ngfr+ glial cell activation is reversed after reinnervation. **a)** Representative immunofluorescence analysis of TA muscle cryosection derived from control and denervated muscle at 3- ,7-,15- and 30-days post nerve lesion, stained for Laminin (green)**. b)** Mean CSA from crushed (DEN) TA muscles at the indicated time points. Values represent mean (n=3, Values represent mean ± s.d. *P < 0.05, **P < 0.01, by One Way Anova test.). **c)** Percentage of muscle weight reduction in crushed (DEN) gastrocnemius (GA) muscles at the indicated time points. Values represent mean (n=3 animals/group). **d)** Representative

immunofluorescence analysis of TA muscle cryosection derived from control and denervated muscle at 3- , and 30-days post nerve lesion, stained for Nfl (red), Laminin (green). Nuclei were counterstained with dapi. Scale bar = 100mm**. e)** Ngfr+ cell quantification, shown in the graphs as a percentage of Itga7+Sca1-Ln population, in denervated muscle at 3- and 30-days post nerve lesion (n≥3, Values represent mean ± s.d. **P < 0.01 and; by One Way Anova test). **f)** qPCR analysis for the expression of Tnc, Gdnf, Nrcam, Plp1 and Shh in freshly isolated Ngfr+ cells derived from denervated muscle at 3- and 30-days post nerve lesion (n=3, Values represent mean ± s.d. *P < 0.05 and **P < 0.01; by One Way Anova test).

4.8 Muscle-resident glial cells are activated upon spinal cord lesion and in a mouse model of ALS

The accumulation of Ngfr+ cells in muscle upon denervation suggests a functional relationship between the integrity of NMJs and muscle-resident glial cell activation. In order to investigate if this activation could be present in other conditions characterized by the nerve damage, we analysed a different traumatic damage model, Spinal Cord Injury (SCI), and a progressive pathological denervated model, such as Amyotrophic Lateral Sclerosis (ALS) one.
The presence of Ngfr+ cells was also observed in the mouse model of SCI where the damage was induced by a mechanical lesion of the spinal cord (Figure 13a). Indeed, after 7 days post spinal lesion, the appearance of Ngfr+ cells was observed in TA muscle. We found that in unperturbed muscles Plp1 positive cells are close to the neuron structure stained for Neurofilament (NF-L) that is lost upon nerve injury. However, upon the injury, Plp1+ /Ngfr+ cells were found in a structure reminiscent of the nerve structure (Figure 13a). Finally, Tnc protein expression and localization close to the NMJ was observed in the TA muscle at 7 days following spinal cord injury (Figure13b).

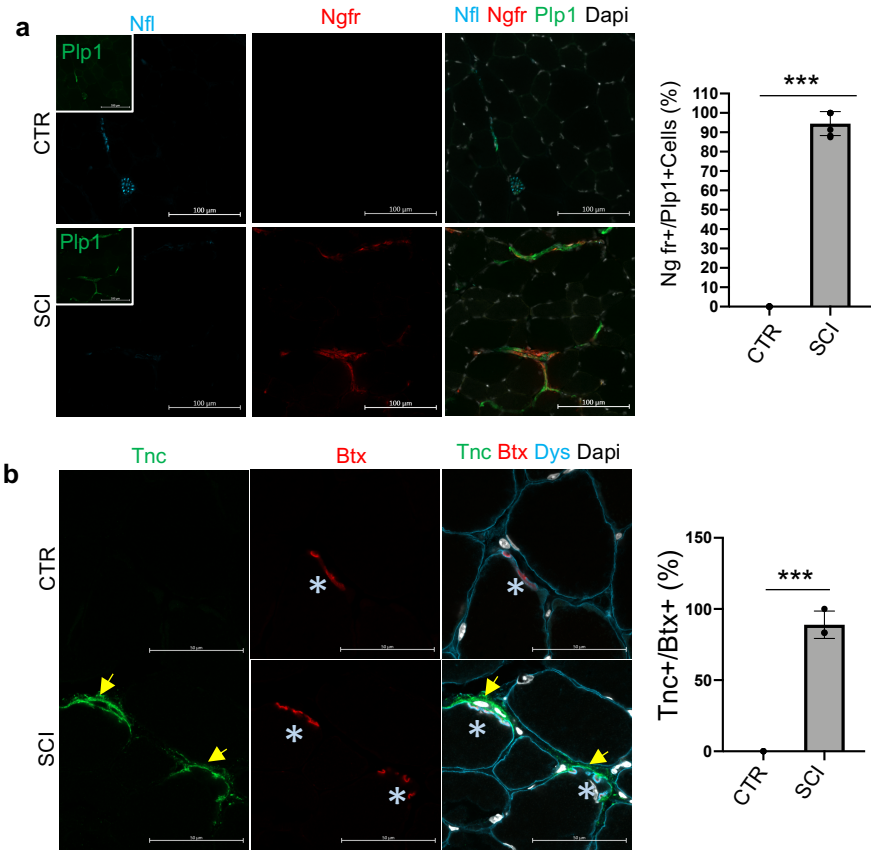

Figure 13 Ngfr+ glial cell activation occurs, also, after spinal cord injury (SCI). **a)** Representative immunofluorescence analysis of control and SCI mice muscle cryosection, at 7-days post injury, stained for Neurofilament-L (Nfl, Cyan), Ngfr (red) and Plp1 (green). Nuclei were counterstained with dapi. Scale bar = 100µm. (right) Quantification graph of Ngfr+/Plp1+ cells in control (CTR) and spinal cord injury (SCI) mice muscle (n=6, Values represent mean ± s.d. **P < 0.01; by Mann-Whitney test). **b)** Representative immunofluorescence analysis of control and SCI mice muscle cryosection, at 7-days post injury, stained for Tnc (green), Bungarotoxin (Btx, red) and Dystrophin (Dys, Cyan). Nuclei were counterstained with dapi. Scale bar = 100µm. Quantification data on the right (n=3, Values represent mean ± s.d. ***P < 0.001; by student t-test).

The symptomatic stage of ALS is characterized by muscle denervation. Motoneuron degeneration leads to muscle atrophy and muscle weakness, ultimately accelerating disease progression. It is currently unclear whether the disease progression could be influenced by the neurotrophic activity of specialized cell types. We, therefore, set to determine whether an increased amount of muscle resident Plp1+/Ngfr+ glial cells could be observed at sequential stages of disease progression, using the $SOD1^{G93A}$ mouse model of ALS.

Indeed, Ngfr expression and Ngfr+ cells among Itga7+ cells increased with disease progression (Figure 14a-c). Ngfr expression displayed a striking increase in muscle derived from symptomatic $SOD1^{G93A}$ at 90- and 140-days of postnatal life with a concomitant reduction of NF-L positive neurofilament in accordance with the progressive loss of muscle innervation (Figure 14b). Other factors such as Gdnf or Tenascin C also increased significantly in $SOD1^{G93A}$ in the late stage of the disease (140d) compared to age-matched healthy animals (Figure 14d). Overall, these observations clearly identify muscle glial cells as potential players in the maintenance of nerve to muscle contact in the context of ALS. Interestingly, the magnitude of the induction of Tnc and Gdnf is clearly lower compared to acute denervation shown in Figure 10. This may account for the reduced reinnervation ability of SOD^{G93A} leading to muscle paralysis that marks the end-stage of the disease. In addition to the lower expression of Tnc compared to reversible nerve degeneration, we also observed a marked difference in Tnc localization in ALS muscle. Indeed, while in reversible denervation we observed a clear localization of Tnc protein close to the NMJ, in SOD^{G93A} muscle Tnc signal encircled muscle fibers without the NMJ associated pattern (Figure 14e). These data suggest a defect in the response of glial cells during disease progression.

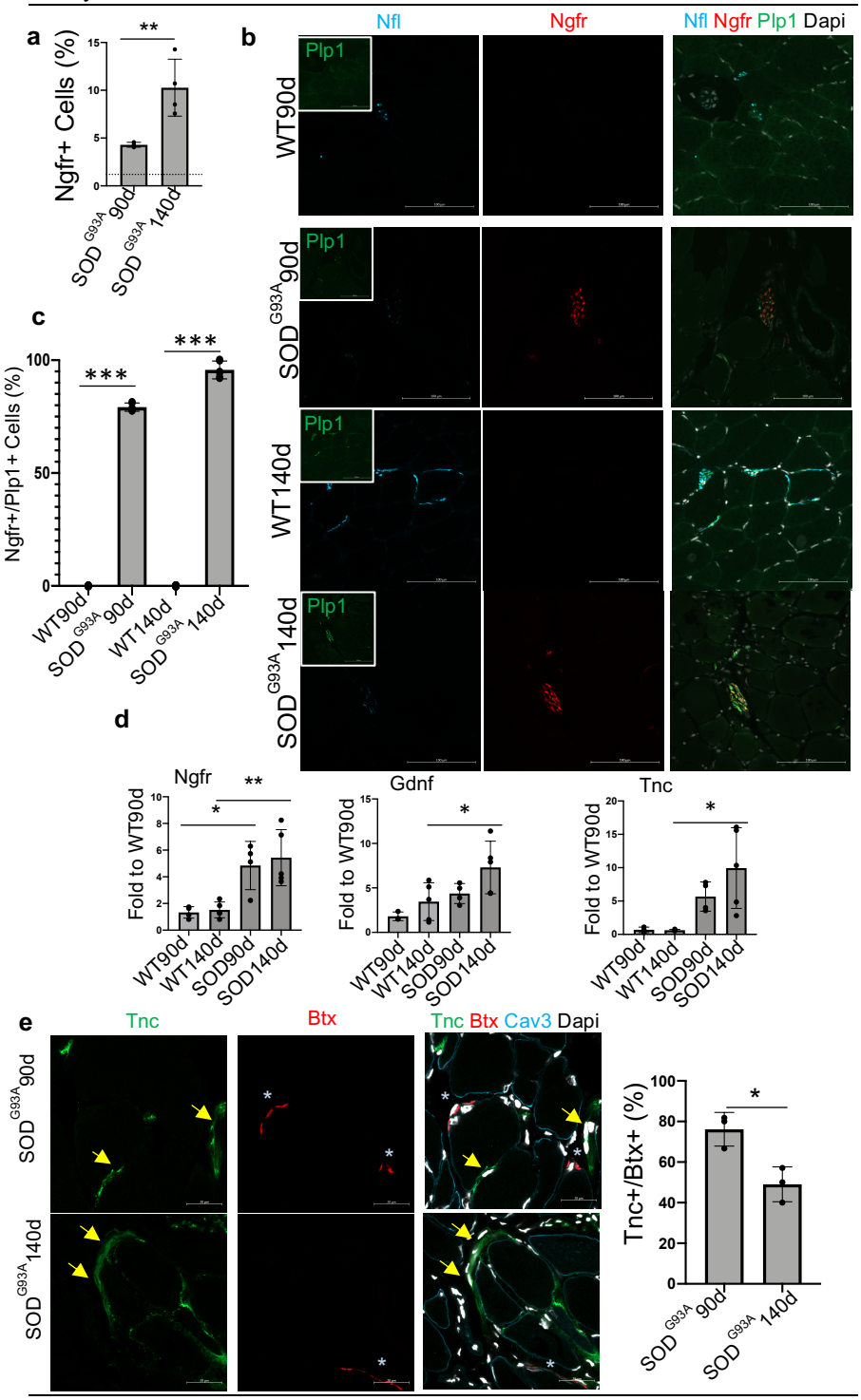
a
Ngfr+ Cells (%)
**
SOD G93A 90d
SOD G93A 140d
b
Nfl
Ngfr
Nfl Ngfr Plp1 Dapi
Plp1
WT90d
SOD G93A 90d
WT140d
SOD G93A 140d
c
Ngfr+/Plp1+ Cells (%)
***
***
WT90d
SOD G93A 90d
WT140d
SOD G93A 140d
d
Ngfr
Gdnf
Tnc
Fold to WT90d
WT90d
WT140d
SOD90d
SOD140d
e
Tnc
Btx
Tnc Btx Cav3 Dapi
SOD G93A 90d
SOD G93A 140d
Tnc+/Btx+ (%)
SOD G93A 90d
SOD G93A 140d

Figure 14 Ngfr+ glial cells accumulate in ALS progression. **a)** Ngfr+ cell cytofluorimetric quantification was shown in the graphs as a percentage of Itga7+Sca1-Ln- population, in 90- and 140-days old SODG93A mice muscle (n=4, Values represent mean ± s.d. **P < 0.01; by One Way Anova test). Dotted line highlight percentage in WT mice muscle. **b)** Representative immunofluorescence analysis of TA muscle cryosection derived from 90- and 140-days old SOD^{G93A} and WT mice stained for Neurofilament-L (Nfl, Cyan), Ngfr (red) and Plp1 (green). Nuclei were counterstained with dapi. Scale bar = 100μm. **c)** Quantification graph of Ngfr+/Plp1+ cells in 90- and 140-days old WT and SOD^{G93A} mice muscle (n=3, Values represent mean ± s.d. ***P < 0.001; by One Way Anova test) **d)** qPCR analysis for the expression of Ngfr, Gdnf and Tnc in freshly isolated Itga7+Sca1-Ln- cells derived from WT and SOD^{G93A} muscle at 90- and 140-days of post-natal life. Gapdh was used as housekeeping gene (n=4, Values represent mean ± s.d. *P < 0.05 and **P < 0.01; by One Way Anova test). **e)** Representative immunofluorescence analysis of TA muscle cryosection derived from 90- and 140-days old SOD^{G93A} and WT mice stained for Tnc (green), Bungarotoxin (Btx, red) and Caveolin-3 (Cav3, Cyan). Arrows highlight Tnc and asterisk highlight Btx. Nuclei were counterstained with dapi. Scale bar = 20μm. (right) Quantification data on the right (n=3, Values represent mean ± s.d. *P < 0.05; by student t-test)

4.9 Muscle-resident glial cells from denervated mice exhibit neurotrophic functional properties

To functionally validate the neurotrophic ability of Plp1+Ngfr+ muscle derived glial cells, we utilized an in-vitro transwell system (Figure 15b). Ngfr+ and Ngfr- cells were isolated from limb muscle of mice subjected to nerve injury or from symptomatic SOD^{G93A}, and co-cultured with the mouse motor neuron-like hybrid cell line (NSC-34), without direct contact through the use of specific trans-well inserts. Following 72h of co-culture in growth media, Ngfr+ cells from denervated muscle promoted NSC-34 neuronal differentiation when compared to control cells cultured under standard neuronal differentiation conditions, as documented by the increase in neurites length and the mean number of neurites per cell (Figure 15a-c). Conversely, this effect was not observed in NSC-34 co-cultured with Ngfr- cells. Interestingly, a lower ability to promote NSC-34 differentiation and neurite elongation was observed in cells co-cultured with Ngfr+ cells derived from SOD^{G93A} muscle (Figure 15a-c).
These data suggest that an impaired ability of muscle-resident glial cells to adopt a neurotrophic phenotype in response to nerve injury could contribute to progressive loss of NMJ in ALS muscles.

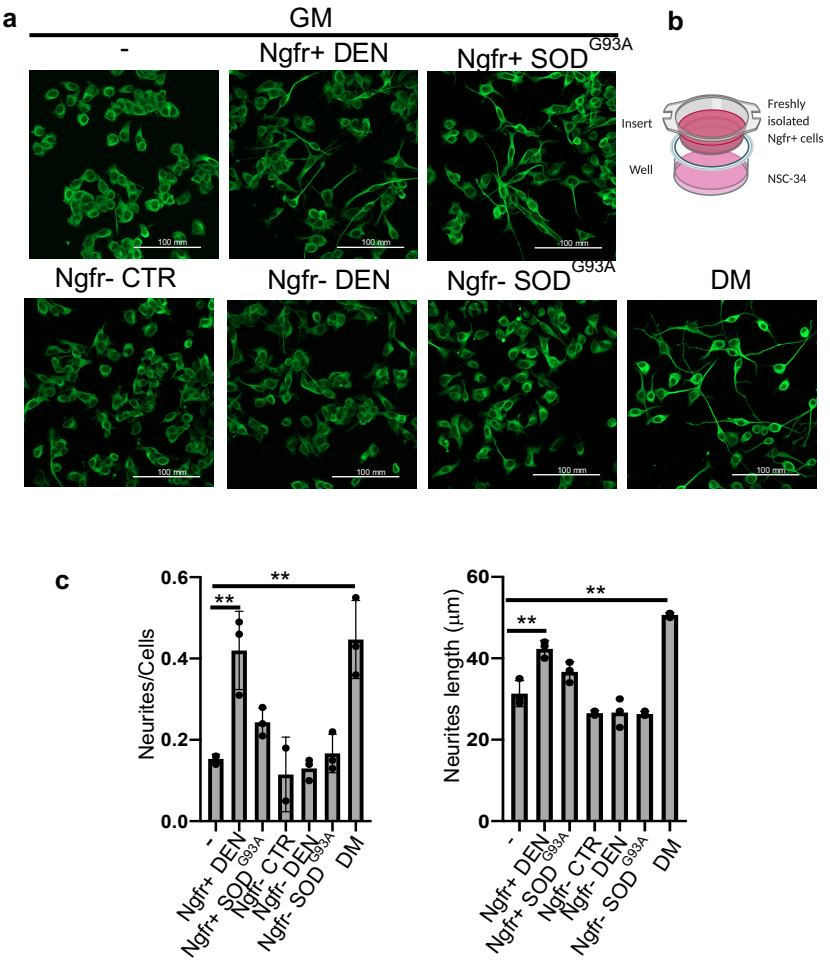

Figure 15 Muscle-resident glial cells promote NSC-34 neuronal differentiation after nerve injury **a)** Representative immunofluorescence analysis of NSC-34 cells in growth media cultured either alone (-) or in co-culture with Ngfr+ or with Ngfr- cells, both from denervated muscle and SOD1^{G93A} muscle at 90-days of post-natal life, and of NSC-34 cells cultured in neurogenic differentiation media (DM), stained for beta-3-Tubulin (green). Scale bar = 100µm. **b)** Schematic representation of in-vitro co-culture system. **c)** Quantification of neurites number per cell and length of NSC-34 cultered in the indicated conditions (n=3, Values represent mean ± s.d. **P < 0.01 and; by One Way Anova test).

5. DISCUSSION

The maintenance of skeletal muscle homeostasis is essential for general health and prevention of disease progression in various neuromuscular conditions. The interactions between myofibres and different cell types that compose the muscle environment, including MuSCs, motor neurons and a variety of interstitial cells, play a crucial role in maintaining this homeostasis.
After muscle damage, the muscle environment changes: the MuSCs, as central players in muscle regeneration, exit from their quiescent state and become activated, while infiltrating immune cells establish functional interactions with other cell types, including FAPs and MuSCs, to promote myofibril regeneration and injury resolution. Recently, scRNA-Seq analysis has been instrumental in unraveling the heterogeneity of muscle-resident cells in unperturbed and regeneration conditions and has been used to reveal the identity of the sub-populations and their trajectories in response to muscle injury (Dell'Orso et al., 2019; Giordani et al., 2019; De Micheli et al., 2020; Oprescu et al., 2020). However, skeletal muscle regeneration is functionally successful only when the motor neurons properly attach to the newly formed myofibers, through the establishment of a new Neuro-Muscular Junction (NMJ). The mechanisms that regulate the growth or extension of neurites toward regenerating fibres and the timing of functional synaptic contact on a fibre remain unclear and unexplored. Earlier studies indicated a contribution of MuSCs in the maintenance of NMJ integrity and regeneration (Liu et al., 2015b, 2017), but the precise identity of the cell types activated by nerve injury and their potential neurotrophic activity remain unknown.

Unlike muscle injury, nerve injury does not promote muscle regeneration but elicits severe myofiber atrophy and muscle fibrosis, which are frequently associated with skeletal muscle dysfunction observed in the context of neuromuscular diseases and aging. Following denervation and loss of NMJ, in early stages, myofibres and different cell types that compose the muscle environment change their gene expression profile and their functional

interactions. For instance, we have previously showed that FAPs are activated in denervated muscles, in the absence of concomitant infiltration of macrophages. Transcriptome analysis revealed a persistent activation of IL6/STAT3 signaling in FAPs from denervated muscle, which promotes myofiber atrophy (Madaro et al., 2018c). These results suggest a different environment and activation of multiple cell types following denervation, compared to the regeneration milieu. At the same time, the selective response of muscles to denervation might help to capture specific muscle-resident cells activated by nerve injury, without the potentially confounding co-existence of other activated cell types following muscle injury.

In this study, we describe a population of muscle-resident glial cells that are activated by nerve injury and might contribute to NMJ repair. These cells express Itga7 - a cell surface protein commonly used to prospectively isolate MuSCs (Pasut et al., 2013). Indeed, a recent study identified a population of smooth muscle mesenchymal cells (SMMCs) within the Itga7+ cells that are also distinct from MuSCs (Giordani et al., 2019). Initially, in our work, we isolated the Itga7+ cells, from control and denervated muscle, by FACS and using a commercial kit (described as tool to isolate muscle satellite cells). Interestingly, both these strategies could not distinguish the Itga7+ myogenic populations from the glial cells due to the common antigen surface marker. Indeed, by using a single-cells RNA sequencing we characterized the Itga7+ cells heterogenicity Interestingly, our results indicated that muscle-resident glial cells, which share with MuSCs and SMMCs the Itga7 expression of Itga7, was the main population that activates the neurotrophic program upon denervation. These cells exhibit a distinctive gene expression signature that is enriched in glial cell-specific genes. While some glial lineage-identity marker was constitutively expressed and could be used for their prospective isolation in unperturbed muscles (Plp1), a subset of neurotrophic genes was selectively expressed in these cells only in response to nerve injury. Among them, Ngfr was instrumental to further isolate the fraction of Itga7/Plp1 glial cells activated upon nerve injury

(Figure10). The Ngfr is a receptor commonly associated with activated glial cells. Since Ngfr expression in Itga7-positive muscle glial cells is only observed upon their activation by nerve injury and coincides with the activation of the neurogenic program, it is conceivable that Ngfr confers upon glial cells the competence to respond to neurogenic signals. The activated muscle glial cells adopt a neurogenic gene expression profile and functional neurotrophic properties. Interestingly, activated muscle glial cells localize close to NMJs. To understand if these muscle glial cells are the activated Perysinaptic Schwann Cells (PSCs) or different muscle resident glial cells, further investigations are needed. A comparative analysis using the RNAseq profiles of Ngfr+ cells isolated either from nerves or from muscles at 3 days post nerve injury revealed clear differences in gene expression between these two populations, suggesting that they might represent two distinct population or two different functional states of glial cells. Nevertheless, the differential expression of certain genes, such as Tnc, Gdnf and Shh, suggests that muscle-resident glial cells adopt different functional phenotypes in response to nerve injury, compared to the glial cells in the nerve.

The upregulation of Tnc in muscle-resident glial cells activated by nerve injury has not been shown previously, and highlights a fundamental difference between the skeletal muscle response to nerve injury versus myotrauma, in which Tnc is typically expressed by other types of resident-muscle cells (e.g. FAPs) and accumulates within the ECM to regulate MuSC activity(De Micheli et al., 2020; Oprescu et al., 2020; Pawlikowski et al., 2019; Tierney et al., 2016). Interestingly, Tnc accumulates in close proximity to bungarotoxin (BTX)-positive NMJ of denervated muscles. Thus, higher levels of Tnc in muscle-derived glial cells and its anatomical localization in proximity of NMJ are distinctive features of skeletal muscle response to NMJ injury. Considering that genetic ablation of Tnc causes delay in NMJ recovery in-vivo (Cifuentes-Diaz et al., 2002), we speculate that muscle glial-cell derived Tnc could contribute to NMJ repair following injury. This possibility is also supported by

the finding that Tnc expression was reduced upon recovery of NMJ integrity (e.g. up to 30 days after lesion).
While it is tempting to speculate on the potential repair of denervation-activated muscle resident glial cells, further studies are necessary to determine whether these cells represent vestigial structures or are effective cellular effectors of nerve repair. Regardless, these cells might be amenable to pharmacological manipulation to facilitate nerve repair in muscles subjected to traumatic injury. Likewise, pharmacological activation of the neurotrophic potential of muscle resident glial cells could be exploited in neurodegenerative disorders, such as ALS. A role for peripheral glial cells in ALS – and in particular pre-synaptic Schwann cells - has been recently suggested, although the precise mechanism of their involvement remains unknown(Arbour et al., 2017; Lasiene and Yamanaka, 2011). In this regard, we found a progressive increase of muscle resident glial cells in muscles of ALS mouse model - $SOD1^{G93A}$ mice. However, activated muscle glial cells from symptomatic $SOD1^{G93A}$ mice exhibited reduced activation of neurotrophic genes, defective Tnc localization and impaired ability to promote neurite outgrowth and differentiation of a motoneuron cell line, compared to glial cells activated in the context of acute reversible denervation. These data suggest that defective activity of muscle-glial cells could contribute to the pathogenesis of neurodegenerative diseases, such as ALS.
Overall, our results, together with those described in literature, suggest a more universal thinking: when a biological system is damaged, it goes into crisis and a change is required from the various components of the system to restore the balance or find a new one. If this does not happen, the system will tend to degenerate gradually. Understanding which of these components comes into play and how, will allows us to intervene in order to improve the system's condition.

6. MATHERIALS AND METHODS

6.1 Mouse Lines

Mouse lines used in this study were:

- C57BL/6J were provided by the Jackson Laboratory (Bar Harbor, USA).
- PAX7CreER/tdTomato$^{f/f}$ mice were provided by the SBP Animal Facility (La Jolla).
- Hemizygous transgenic mice carrying the mutant human SOD1^{G93A}(B6.Cg-Tg(SOD1*G93A)1Gur/J) gene were originally obtained from Jackson Laboratories (Bar Harbor, USA).
- CD1 were provided by Charles River Laboratories, Como, Italy.

All mice were maintained in a pathogen-free animal facility under standard 12h light/12h dark cycle at 21 °C with access to red house and to standard chow and water ad libitum. Three-month-old mice were used for ex-vivo experiments, except for the SOD1^{G93A} mice, as indicated in the Figure 14. Both male and female mice were used in the denervation experiment of C57BL/6J and PAX7CreER/tdTomato$^{f/f}$ mice. Female mice were used for spinal cord injury experiment. Male SOD1^{G93A} mice were used as a mouse model for ALS.

6.2 Cell Lines and Primary Cell Cultures

We used mouse MN-like NSC-34 cells, which is a hybrid cell line produced by the fusion of MNs from the spinal cord embryos with N18TG2 neuroblastoma cells (Cashman et al., 1992) that exhibit properties of MNs after differentiation and maturation protocols. Thus, NSC-34 cells were grown in proliferation media [Dulbecco's Modified Eagle Medium:Nutrient Mixture *F-12* (*DMEM* / *F-12*- Sigma-Cat # D6421) supplemented with 10% of fetal bovine serum

(FBS- Sigma- Cat # F4135) and 1% of Penicillin/Streptomycin (Gibco- Cat # 15070-063)]. Cells were maintained at 37°C in a humidified atmosphere of 5% CO_2. Differentiation was induced by changing medium for DMEM-F12 plus 0.5% of FBS, 1% of non-essential amino acids (NEAA- Thermo Fisher- Cat # 11140050), 1% of Penicillin/Streptomycin.
Primary mouse Ngfr+ cells isolated from denervated mice were used for co-culture experiments.
NSC-34 and Ngfr+ cells were used for co-culture experiments.

6.3 Denervation

Unilateral hindlimb denervation was performed by clamping the left sciatic nerve under anesthesia by intraperitoneal injection of 40 mg/kg ketamine (Zoletil® - Virbac) and 10 mg/kg xylazine (Rampum- BAYER). Upon exposure of the sciatic nerve, the nerve was crushed for three times for 10 seconds. Alternative, for the bulk RNA-seq in Figure 6a, nerve was cut with a scissor. The lesion was sutured after the operation.

6.4 Spinal cord injury

Three-month-old CD1 mice (Charles River Laboratories or EMMA InfraFrontiers) were used in SCI. To perform SCI, mice were deeply anaesthetized, the back hairs were shaved, the skin was disinfected with betadine, and an incision was made to expose the spinal cord. Animals were mounted on a stereotaxic apparatus with spinal adaptors connected to a cortical PinPoint precision impactor device (Stoelting) and maintained at 37 °C throughout surgery. To induce a severe trauma the following parameters were set up: middle, round and flat tip (#4); velocity 3 m s^{-1}; depth 5 mm; dwell time 800 ms. The impact was applied at the thoracic level (vertebrae T10–T11). Analysis of the graphical impact parameters, operated by the PinPoint software, was used to identify potential outliers. Behavioural analyses were also used to corroborate differences in

injury severity within groups. Slight lesions were excluded from the study based on these criteria.

6.5 Cell preparation and isolation by FACS

Tibialis anterior and gastrocnemius muscles, or nerves, of mice were subjected to enzymatic dissociation [in PBS (gibco- Cat # 14040-091) with 2 mg/mL Collagenase A (Roche- Cat # 10 103 586 001), 2,4 U/mL Dispase I (Roche- Cat # 04 942 078 001), 10 ng/mL DNase (SIGMA- Cat #11 284 932 001), 0,4 mM $CaCl_2$ and 5mM $MgCl_2$] for 60 min at 37° C. The cell suspension was filtered through a 40-μm nylon filter and incubated with the following antibodies for 30 min: CD45, CD31, TER119, Sca1 and α7-integrin (Itga7).
Ngfr+ cells were isolated as TER119–/CD45–/CD31–/Itga7+/SCA-1–/Ngfr+ cells and Pax7-Tomato + as TER119–/CD45–/CD31–/Itga7+/SCA-1–/Tomato+ .
In Figure 6d, satellite cell purification was performed by using SC Isolation Kit (Miltenyi Biotech, Bergisch Gladbach, Germany- Cat # 130-104-268).

6.6 Histology Immunofluorescence

For the histological analysis 8 μm muscle cryosection were analysed. Both cryosections and cultured cells were fixed in 4% PFA for 10 min and permeabilized with 100% acetone for 1 min at RT or with 0.1% Triton for 15 min at RT. Muscle sections and cultured cells were then blocked for 1h with a solution containing 4% BSA (Sigma - Cat # A7030-100G) in PBS (gibco- Cat # 14190-094). PAX7 staining was performed by an antigen retrieval protocol. The primary antibodies immunostaining was performed ON at 4°C and then the antibody binding specificity was revealed using secondary antibodies coupled to Alexa Fluor 488, 594, or 647 (Invitrogen). Acetylcholine receptors (AChRs) were revealed with fluorescently labeled Bungarotoxin (BTX) (1:500 Alexa 594, Invitrogen). Sections were incubated with DAPI in PBS for 5

minutes for nuclear staining, washed in PBS, and mounted with mounting medium or glycerol (3:1 in PBS).
The primary antibodies used for immunofluorescences are: rabbit anti-Plp1 (1:100); mouse anti NFl (1:200); rat anti-Ngfr-PE (1:100); rabbit anti-Tnc (1:100); mouse anti-Caveolin-3 (1:1000); rabbit anti-Laminin (1:400); anti BIII-Actin (1:500); mouse anti-PAX7 (Developmental Studies Hybridoma Bank, DSHB, 1:20); mouse anti-Myosin (1:10); mouse αTubulin (1:200).
The transverse sections and cultured cells were visualized on a Zeiss confocal microscope then edited using the ImageJ® software. All histological analysis were performed blind to treatment group by investigator.
The figures reported are representative of all the examined fields.

6.7 EdU Proliferation Assay

Cell proliferation was measured by EdU incorporation. 20 mg per kg body weight EdU was administered intraperitoneally (i.p.) 12h before muscle harvest. Incorporation of EdU was revealed using the "Click-iT™ EdU Cell Proliferation Kit for Imaging, Alexa Fluor™ 594 dye" (Thermo Fisher- Cat # C10354) following the manufacture protocol.

6.8 Cell culture procedures

All cells were cultured in incubators at 37 °C and 5% CO_2. Freshly isolated MuSCs and Ngfr+ cells were plated in 24-well plates in GM [DMEM [+Pyruvate](Thermo Fisher- Cat # 10569010), 20% fetal bovine serum (FBS), 10% Hourse Serum (Gibco-Cat #26050-070) , 1% Chick Embryo Extract (CEE – Seralab – Cat # CE-650-F)]. Myogenic differentiation was induced with DMEM and 2% horse serum for 2 or 3 days.

6.9 Co-culture conditions of Ngfr+ cells and NSC34

NSC-34 and Ngfr+ cells were cocultured by using inserts with 1μm porous membrane to avoid direct contact between populations. NSC-34 were grown independently from Ngfr+ in proliferation media for 48h in 24-well plates. After 24h, freshly sorted Ngfr+ cells were plated on the upper insert and transwell co-cultures were maintained for additional 72h in proliferation and differentiation media.

6.10 RNA analysis by quantitative PCR

RNA was extracted from cells using Qiagen RNeasy mini-kits (Qiagen - Cat # 74106) following the manufacturer's protocol. Total RNA was quantified with a Nanodrop 8000 spectrophotometer (Thermo Scientific, Wilmington). First-strand cDNA was synthesized from total RNA using the Transcriptor First Strand cDNA Synthesis kit (Roche - Cat # N808-0234) following the manufacturer's protocols. The generated cDNA was used as a template in real-time PCR reactions with Lightcycler 480 SYBR Green 1 master mix (SMOBIO - Cat # TQ1211) and was run on a Roche LC480 machine using three-step amplification and melt curve analysis. Quantitative real-time PCR reactions consisted of 2× SYBR Green Supermix, 0.25 mmol l^{-1} forward and reverse primers and 10 ng cDNA. Relative gene expression was normalized by dividing the specific expression value by the glyceraldehyde 3-phosphate dehydrogenase (Gapdh) expression value and calculated using the $2^{-\delta\Delta CT}$ method.

6.11 Tamoxifen (Tmx) treatment and denervation

We used *Pax7CreER ™ ;R26R^{TdT}* mice between the ages of 2 and 3 mouth for Tmx (Sigma- Cat # T5648) injections. Tmx (3 mg) suspended in corn oil was injected intraperitoneally (i.p.) each day for 5 d. After 7 d from the last injection, we performed the unilateral hindlimb denervation. Tissues were harvested after 3 d for FACS.

6.12 RNA-sequencing

MuSC were isolated from mice TA and GA muscle as described. RNA from MuSC was extracted using RNeasy Mini kit (Qiagen) following the manufacturer's protocol. RNA was shipped to the sequencing IGA of Udine. The libraries for sequencing were prepared using NuGEN Ovation System V2 RNA-Seq. For each biological sample two independent experiments were carried out for the isolation of RNA. All duplicates are pool of three different mice, sorted at different times.

6.13 RNA-sequencing data processing

For sequencing alignment we used the human reference genome assembly GRCm38/mm10 (http://ftp.ensembl.org/pub/release-76/fasta/ mus_musculus/dna/), and for transcriptome annotation we used version 85 of the GRCm38 (http://ftp.ensembl.org/pub/release85/gtf/mus_musculus/Mus_musculus. GRCm38.85.gtf.gz). We used the FASTQC package (v0.11.3) to assess the quality of sequenced libraries. All passed quality control. Reads were mapped to the reference genome using TopHat2 v.2.1.1. The quality control of the reads distribution along transcripts was performed using infer_experiment.py from RSeQC package v2.6.3. All samples had a uniform distribution of reads along transcripts. The sequenced read counts per annotated gene were derived with the use of htseq-count script distributed with HTSeq v0.5.4p5. We used the R library package DESeq2 v.1.12.4 for measuring differential gene expression between two different cell conditions, considering the two RNA–seq experiments as biological replicates. We picked genes with adjusted P value < 0.001. Gene ontology analysis was performed using David 6.8 (https://david.ncifcrf.gov/). In details Biological Process was predicted on genes differentially expressed with p adjusted<0.01 with the following setting: threshold counts=2, threshold EASE=0.1. The most significant 12 functional annotation was illustrated in the figure.

6.14 Single-cell RNA-sequencing

Single-cell RNA-sequencing was performed at IGA facility of Udine - Italy (https://igatechnology.com/). Methanol fixed cells were rehydrated following 10X Genomics recommendation. In order to remove visible debris, an additional washing in Wash-Resuspension buffer was introduced. Cell concentration was determined using the Countess II FL Automated Cell Counter (Thermo Fisher Scientific, Waltham, MA). Trypan Blue staining of the methanol fixed cells showed that 100% of the cells were dead, indicating that all cells were effectively fixed and permeabilized.
Chromium controller and Chromium NextGEM Single Cell 3' Reagents Kit v3.1 (10X Genomics, Pleasanton, CA) have been used for partitioning cells into Gel Beads-in-emulsion (GEMs), where all generated cDNA share a common 10x barcode. Libraries were generated from the cDNA following manufacturer's instruction and checked with both Qubit 2.0 Fluorometer (Invitrogen, Carlsbad, CA) and Agilent Bioanalyzer DNA assay (Agilent technologies, Santa Clara, CA). Libraries were then prepared for sequencing and sequenced on NovaSeq6000 (Illumina, San Diego, CA) with the following run parameters: Read 1=28 cycles, i7 index=8 cycles, Read 2=91 cycles.

6.15 Single-cell RNA-sequencing data processing

The raw sequencing data were processed by Cell Ranger v 3.1.0 (10X Genomics) with mouse transcriptome reference mm10 to generate gene-cell expression matrices. Further data analysis was carried out in R version 3.6.0 using Seurat version 3.1.1 (Butler et al., 2019). The two datasets were set up as independent Seurat objects. ''Cells''that fit any of the following criteria were filtered out: < 200 or > 4,500 expressed genes, or > 10% UMIs mapped to mitochondria. Dataset normalization and identification of variable features were performed using the NormalizeData() function and the FindVariableFeatures() with following parameters (selection.method = "vst", nfeatures = 4000). Integration anchors

were computed using the first 20 dimensions, using all the genes present in both datasets as features to integrate. Finally, we obtained 3949 cells that passed quality control, with an average of 1,460 genes expressed per cell. For downstream integrated analyses, top 30 components were used for PCA, UMAP and cluster identification (using a resolution of 0.4). Further, we manually assigned cell population identity based on cell-type-specific markers and merged those clusters that displayed similar canonical markers. After clustering and cell population identification, the most highly differentially expressed genes, or putative cluster markers, were identified by a likelihood-ratio test using the FindAllMarkers() function with the following parameters(only.pos = TRUE, min.pct =0.5, min.diff.pct=0.25, logfc.threshold = 0.25). Genes differentially expressed in CTR vs DEN where identified using the FindMarkers() function and subsequently filtered using the following criteria (pct.1>0.45 or pct.2>0.45; p_val_adj<0.01; avg_logFC< (-0.58) or avg_logFC>0.58).

6.16 Figure Design

Figure 3 and Figure 4 were created with BioRender (https://biorender.com/)

6.17 Statistics

Data are presented as mean with SD. Statistical analysis was performed using Graph Pad Prism 8.0 software (Pad Software).
For all the statistical analyses, normality test (Shapiro-Wilk) is used to verify the normal distribution of the samples. If the values follow a Gaussian distribution, we used the unpaired two-tailed Student's t test to compare the means of two groups, while if the test failed, then we used a non-parametric analysis (Mann–Whitney) to test the null hypothesis between the two groups. One-way ANOVA with Tukey's test was used for comparison three or more unmatched groups. The specific test used in all the comparisons is indicated in the figure legends. Significance was defined as $P < 0.05$ (*), $P < 0.01$ (**), and $P < 0.001$ (***).

The number of biological replicates for each experiment is indicated in the figure legends. RNAseq data was performed in 2 independent samples derived from different animals. Statistical method was Deseq2. Right-tailed Fisher's exact test and one-sided Fisher's exact test was used for IPA analyses. For scRNA-seq, biological sample replicates came also from separate mice. Histological and Immunofluorescence images are representative of at least 3 different experiment/animals. For cell culture studies, biological replicates from separate culture wells.

6.18 Data and code availability

Details of the material and reagents used can be found in the supplemental material.
a7int+ mouse bulk RNA-sequencing data will available at the SRA repository before publication. The data it is already available for reviewer at the following link:
https://dataview.ncbi.nlm.nih.gov/object/PRJNA623246?reviewer=979m70qhb9i5d61eh99q9rn63a

Mouse Single Cells RNA-sequencing data will available at the SRA repository before publication. The data it is already available for reviewer at the following link:
https://dataview.ncbi.nlm.nih.gov/object/PRJNA626530?reviewer=gfkrd8gmfuaf0e08u9imlq5d56

Ngfr+ Mouse bulk RNA-sequencing data will available at the SRA repository before publication. The data it is already available for reviewer at the following link:
https://dataview.ncbi.nlm.nih.gov/object/PRJNA649152?reviewer=dul096h0124er7c5krd7lb0o2i

STUDY APPROVAL

All experiments in this study were performed in accordance with protocols approved by Italian Ministry of Health, National Institute of Health (IIS), and Santa Lucia Foundation (Rome) and by the Sanford Burnham Prebys Medical Discovery Institute Animal Care and Use Committee. The study is compliant with all relevant ethical regulations regarding animal research and in the respect of the principles of the 3Rs (Replacement, Reduction and Refinement).

ANTIBODIES		
NAME	SOURCE	IDENTIFIER
Anti-Mouse CD31 (PECAM-1) PB eBioscience™ (1:50 for FACS)	Invitrogen	Cat # 48-0311-82
Anti-Mouse CD45 PB eBioscience™ (1:50 for FACS)	Invitrogen	Cat # 48-0451-82
Anti- Mouse TER119 PB eBioscience™ (1:50 for FACS)	Invitrogen	Cat # 48-5921-82
Anti- Mouse Ly-6A/E (Sca1) FITC eBioscience™ (1:50 for FACS)	Invitrogen	Cat # 11-5981-82
Anti-α7-Integrin 647 (1:500 for FACS)	AbLab	Cat # AB0000850 6048228060
CD271 (LNGFR)-PE human and mouse (1:50 for FACS and IF)	Miltenyi Biotec	Cat # 130-118-793
Anti-Plp1 (1:100 for IF)	Cell Signaling	Cat # 28702S
Anti-Nfl (1:200 for IF)	Santa Cruz Biotechnology	Cat # SC-20012
Anti-βIII- Tubulin mAb (1:500 for IF)	PROMEGA	Cat # G712A
Anti-Tnc (1:100 for IF)	EMD Millipore Corp.	Cat # AB19013
Anti-Caveolin-3 (1:1000 for IF)	BD Trasduction Laboratories	Cat # 610420
Anti-Laminin (1:400 for IF)	Sigma	Cat # L9393

Anti-Pax7 (1:20 for IF)	Developmental Studies Hybridoma Bank, DSHB	
Anti-Myosin (1:10 for IF)	Developmental Studies Hybridoma Bank DSHB, MF20	
α-Tubulin (1:200 for IF)	Cell Signaling,	Cat #2144
Rabbit polyclonal anti-Laminin	Sigma-Aldrich	Cat # L9393
Bungarotoxin 594 and 488 coniugated	Invitrogen	Cat # B13423 and B13422
Goat anti-Mouse Alexa Fluor 647 (1:400 for IF)	Invitrogen	Cat # A32728
Goat anti-Rabbit Alexa Fluor 488 (1:400 for IF)	Invitrogen	Cat # A32731
Goat anti-Mouse Alexa Fluor 488 (1:400 for IF)	Invitrogen	Cat # A32723
Goat anti-Mouse Alexa Fluor 594 (1:400 for IF)	Invitrogen	Cat # A32742

PRIMERS	
Gapdh FW	CACCATCTTCCAGGAGCGAG
Gapdh RV	CCTTCTCCATGGTGGTGAAGAC
Ngfr FW	TGCCTGGACAGTGTTACGTT
Ngfr RV	ACAGGGAGCGGACATACTCT
Shh FW	CACCCCCAATTACAACCCCG
Shh RV	CTTGTCTTTGCACCTCTGAGTC
Fgf5 FW	CTGTACTGCAGAGTGGGCAT
Fgf5 RV	AATTTGGCTTAACACACTGGC
Runx2 FW	GCCTTCAAGGTTGTAGCCCT
Runx2 RV	GTTCTCATCATTCCCGGCCA
Olig1 FW	CTCGCCCAGGTGTTTTGTTG
Olig1 RV	TAAGTCCGAACACCGATGGC

Tnc FW	CTACCACAGAGGCCTTGCC
Tnc RV	AGCAGCTTCCCAGAATCCAC
Pax7 FW	AGGACGACGAGGAAGGAGACA
Pax7 RV	TCATCCAGACGGTTCCCTTT
Vcam1 FW	GCACTCTACTGCGCATCTT
Vcam1 RV	CACCAGACTGTACGATCCT
Nrcam FW	ATGCACAGACATCAGTGGGG
Nrcam RV	GCTTGCCATTGCCTTCTTACC
Gdnf FW	TGGGTCTCCTGGATGGGATT
Gdnf RV	CGGCGGCACCTCGGAT
Plp1 FW:	CCTAGCAAGACCTCTGCCAGTA
Plp1 RV:	GGACAGAAGGTTGGAGCCACAA

7. REFERENCES

Arbour, D., Vande Velde, C., and Robitaille, R. (2017). New perspectives on amyotrophic lateral sclerosis: the role of glial cells at the neuromuscular junction. J. Physiol. *595*, 647–661.

Barik, A., Lu, Y., Sathyamurthy, A., Bowman, A., Shen, C., Li, L., Xiong, W.C., and Mei, L. (2014). LRP4 is critical for neuromuscular junction maintenance. J. Neurosci. *34*, 13892–13905.

Bentzinger, C.F., Wang, Y.X., Dumont, N.A., and Rudnicki, M.A. (2013). Cellular dynamics in the muscle satellite cell niche. EMBO Rep. *14*, 1062–1072.

Biferali, B., Proietti, D., Mozzetta, C., and Madaro, L. (2019). Fibro–Adipogenic Progenitors Cross-Talk in Skeletal Muscle: The Social Network. Front. Physiol. *10*, 1074.

Bodine, S.C. (2001). Identification of Ubiquitin Ligases Required for Skeletal Muscle Atrophy. Science (80-.). *294*, 1704–1708.

Bodine, S.C., Stitt, T.N., Gonzalez, M., Kline, W.O., Stover, G.L., Bauerlein, R., Zlotchenko, E., Scrimgeour, A., Lawrence, J.C., Glass, D.J., et al. (2001). Akt/mTOR pathway is a crucial regulator of skeletal muscle hypertrophy and can prevent muscle atrophy in vivo. Nat. Cell Biol. *3*, 1014–1019.

Bonaldo, P., and Sandri, M. (2013). Cellular and molecular mechanisms of muscle atrophy. Dis. Model. Mech. *6*, 25–39.

Bouchè, M., Lozanoska-Ochser, B., Proietti, D., and Madaro, L. (2018). Do neurogenic and cancer-induced muscle atrophy follow common or divergent paths? Eur. J. Transl. Myol. *28*, 7931.

Brack, A.S., and Rando, T.A. (2012). Tissue-specific stem cells: Lessons from the skeletal muscle satellite cell. Cell Stem Cell *10*, 504–514.

Cappello, V., and Francolini, M. (2017). Neuromuscular junction dismantling in amyotrophic lateral sclerosis. Int. J. Mol. Sci. *18*.

Chai, R.J., Vukovic, J., Dunlop, S., Grounds, M.D., and Shavlakadze, T. (2011). Striking denervation of neuromuscular junctions without lumbar motoneuron loss in geriatric mouse muscle. PLoS One *6*.

Chal, J., and Pourquié, O. (2017). Making muscle: Skeletal myogenesis in vivo and in vitro. Dev. *144*, 2104–2122.

Chargé, S.B.P., and Rudnicki, M.A. (2004). Cellular and Molecular Regulation of Muscle Regeneration. Physiol. Rev. *84*, 209–238.

Chen, G., Ning, B., and Shi, T. (2019). Single-cell RNA-seq technologies and related computational data analysis. Front. Genet. *10*.

Chiu, A.Y., Zhai, P., Dal Canto, M.C., Peters, T.M., Kwon, Y.W., Prattis, S.M., and Gurney, M.E. (1995). Age-dependent penetrance of disease in a transgenic mouse model of familial amyotrophic lateral sclerosis. Mol. Cell. Neurosci. *6*, 349–362.

Cifuentes-Diaz, C., Faille, L., Goudou, D., Schachner, M., Rieger, F., and Angaut-Petit, D. (2002). Abnormal reinnervation of skeletal muscle in a tenascin-C-deficient mouse. J. Neurosci. Res. *67*, 93–99.

Collins, C.A., Olsen, I., Zammit, P.S., Heslop, L., Petrie, A., Partridge, T.A., and Morgan, J.E. (2005). Stem cell function, self-renewal, and behavioral heterogeneity of cells from the adult muscle satellite cell niche. Cell *122*, 289–301.

Couesnon, A., Offner, N., Bernard, V., Chaverot, N., Backer, S., Dimitrov, A., Perez, F., Molgó, J., and Bloch-Gallego, E. (2013). CLIPR-59: A protein essential for neuromuscular junction stability during mouse late embryonic development. Dev. *140*, 1583–1593.

Darabid, H., Perez-Gonzalez, A.P., and Robitaille, R. (2014). Neuromuscular synaptogenesis: Coordinating partners with multiple functions. Nat. Rev. Neurosci. *15*, 703–718.

Dell'Orso, S., Juan, A.H., Ko, K.-D., Naz, F., Perovanovic, J., Gutierrez-Cruz, G., Feng, X., and Sartorelli, V. (2019). Single cell analysis of adult mouse skeletal muscle stem cells in homeostatic and regenerative conditions. Development *146*, dev174177.

Deng, H.X., Hentati, A., Tainer, J.A., Iqbal, Z., Cayabyab, A., Hung, W.Y., Getzoff, E.D., Hu, P., Herzfeldt, B., Roos, R.P., et al. (1993). Amyotrophic lateral sclerosis and structural defects in Cu,Zn superoxide dismutase. Science (80-.). *261*, 1047–1051.

Dobrowolny, G., Aucello, M., Rizzuto, E., Beccafico, S., Mammucari, C., Bonconpagni, S., Belia, S., Wannenes, F., Nicoletti, C., Del Prete, Z., et al. (2008). Skeletal Muscle Is a Primary Target of SOD1G93A-Mediated Toxicity. Cell Metab. *8*, 425–436.

Eguchi, T., Tezuka, T., Miyoshi, S., and Yamanashi, Y. (2016). Postnatal knockdown of dok-7 gene expression in mice causes structural defects in neuromuscular synapses and myasthenic pathology. Genes to Cells *21*, 670–676.

Ehmsen, J.T., and Höke, A. (2020). Cellular and molecular features of neurogenic skeletal muscle atrophy. Exp. Neurol. *331*, 113379.

Farup, J., Madaro, L., Puri, P.L., and Mikkelsen, U.R. (2015). Interactions between muscle stem cells, mesenchymal-derived cells and immune cells in muscle homeostasis, regeneration and disease. Cell Death Dis. *6*, e1830–e1830.

Feige, P., Brun, C.E., Ritso, M., and Rudnicki, M.A. (2018). Orienting Muscle Stem Cells for Regeneration in Homeostasis, Aging, and Disease. Cell Stem Cell *23*, 653–664.

Feng, Z., and Ko, C.-P. (2008). The Role of Glial Cells in the Formation and Maintenance of the Neuromuscular Junction. Ann. N. Y. Acad. Sci. *1132*, 19–28.

Fischer, L.R., Culver, D.G., Tennant, P., Davis, A.A., Wang, M., Castellano-Sanchez, A., Khan, J., Polak, M.A., and Glass, J.D. (2004). Amyotrophic lateral sclerosis is a distal axonopathy: Evidence in mice and man. Exp. Neurol. *185*, 232–240.

Frontera, W.R., and Ochala, J. (2015). Skeletal Muscle: A Brief Review of Structure and Function. Behav. Genet. *45*, 183–195.

Geraldo, S., and Gordon-Weeks, P.R. (2009). Cytoskeletal dynamics in growth-cone steering. J. Cell Sci. *122*, 3595–3604.

Giordani, L., He, G.J., Negroni, E., Sakai, H., Law, J.Y.C., Siu, M.M., Wan, R., Corneau, A., Tajbakhsh, S., Cheung, T.H., et al. (2019). High-Dimensional Single-Cell Cartography Reveals Novel Skeletal Muscle-Resident Cell Populations. Mol. Cell *74*, 609-621.e6.

Glass, D.J. (2005). Skeletal muscle hypertrophy and atrophy signaling pathways. Int. J. Biochem. Cell Biol. *37*, 1974–1984.

Gomes, M.D., Lecker, S.H., Jagoe, R.T., Navon, A., and Goldberg, A.L. (2001). Atrogin-1, a muscle-specific F-box protein highly expressed during muscle atrophy. Proc. Natl. Acad. Sci. U. S. A. *98*, 14440–14445.

Le Grand, F., Grifone, R., Mourikis, P., Houbron, C., Gigaud, C., Pujol, J., Maillet, M., Pagès, G., Rudnicki, M., Tajbakhsh, S., et al. (2012). Six1 regulates stem cell repair potential and self-renewal during skeletal muscle regeneration. J. Cell Biol. *198*, 815–832.

Griffin, J.W., and Thompson, W.J. (2008). Biology and pathology of nonmyelinating schwann cells. Glia *56*, 1518–1531.

Grönholdt-Klein, M., Altun, M., Becklén, M., Dickman Kahm, E., Fahlström, A., Rullman, E., and Ulfhake, B. (2019). Muscle atrophy and regeneration associated with behavioural loss and recovery of function after sciatic nerve crush. Acta Physiol. (Oxf). e13335.

Gurney, M.E., Pu, H., Chiu, A.Y., Dal Canto, M.C., Polchow, C.Y., Alexander, D.D., Caliendo, J., Hentati, A., Kwon, Y.W., Deng, H.X., et al. (1994). Motor neuron degeneration in mice that express a human Cu,Zn superoxide dismutase mutation. Science (80-.). *264*, 1772–1775.

Heredia, J.E., Mukundan, L., Chen, F.M., Mueller, A.A., Deo, R.C., Locksley, R.M., Rando, T.A., and Chawla, A. (2013). Type 2 Innate Signals Stimulate Fibro/Adipogenic Progenitors to Facilitate Muscle Regeneration. Cell *153*, 376–388.

Hicks, M.R., Hiserodt, J., Paras, K., Fujiwara, W., Eskin, A., Jan, M., Xi, H., Young, C.S., Evseenko, D., Nelson, S.F., et al. (2018). ERBB3 and NGFR mark a distinct skeletal muscle progenitor cell in human development and hPSCs. Nat Cell Biol *20*, 46–57.

Hwang, B., Lee, J.H., and Bang, D. (2018). Single-cell RNA sequencing technologies and bioinformatics pipelines. Exp. Mol. Med. *50*.

Joe, A.W.B., Yi, L., Natarajan, A., Le Grand, F., So, L., Wang, J., Rudnicki, M.A., and Rossi, F.M. V. (2010). Muscle injury activates resident fibro/adipogenic progenitors that facilitate myogenesis. Nat. Cell Biol. *12*, 153–163.

Kablar, B., and Rudnicki, M.A. (1999). Development in the absence of skeletal muscle results in the sequential ablation of motor neurons from the spinal cord to the brain. Dev. Biol. *208*, 93–109.

Kang, H., Tian, L., and Thompson, W. (2003). Terminal Schwann cells guide the reinnervation of muscle after nerve injury. J. Neurocytol. *32*, 975–985.

Kang, H., Tian, L., Mikesh, M., Lichtman, J.W., and Thompson, W.J. (2014). Terminal schwann cells participate in neuromuscular synapse remodeling during reinnervation following nerve injury. J. Neurosci. *34*, 6323–6333.

Koirala, S., Reddy, L. V., and Ko, C.P. (2003). Roles of glial cells in the formation, function, and maintenance of the neuromuscular junction. J. Neurocytol. *32*, 987–1002.

Kolodziejczyk, A.A., Kim, J.K., Svensson, V., Marioni, J.C., and Teichmann, S.A. (2015). The Technology and Biology of Single-Cell RNA Sequencing. Mol. Cell *58*, 610–620.

Kraft, A.D., Resch, J.M., Johnson, D.A., and Johnson, J.A. (2007). Activation of the Nrf2-ARE pathway in muscle and spinal cord during ALS-like pathology in mice expressing mutant SOD1. Exp. Neurol. *207*, 107–117.

Kummer, T.T., Misgeld, T., and Sanes, J.R. (2006). Assembly of the postsynaptic membrane at the neuromuscular junction: Paradigm lost. Curr. Opin. Neurobiol. *16*, 74–82.

Lasiene, J., and Yamanaka, K. (2011). Glial cells in amyotrophic lateral sclerosis. Neurol. Res. Int. *2011*.

Lemos, D.R., Babaeijandaghi, F., Low, M., Chang, C.-K., Lee, S.T., Fiore, D., Zhang, R.-H., Natarajan, A., Nedospasov, S.A., and Rossi, F.M. V (2015). Nilotinib reduces muscle fibrosis in chronic muscle injury by promoting TNF-mediated apoptosis of fibro/adipogenic progenitors. Nat. Med. *21*, 786–794.

Lepore, E., Casola, I., Dobrowolny, G., and Musarò, A. (2019). Neuromuscular Junction as an Entity of Nerve-Muscle Communication. Cells *8*, 906.

Li, L., Xiong, W.C., and Mei, L. (2018). Neuromuscular Junction Formation, Aging, and Disorders. Annu. Rev. Physiol. *80*, 159–188.
Lin, W., Sanchez, H.B., Deerinckt, T., Morris, J.K., Ellisman, M., and Lee, K.F. (2000). Aberrant development of motor axons and neuromuscular synapses in erbB2-deficient mice. Proc. Natl. Acad. Sci. U. S. A. *97*, 1299–1304.

Liscic, R.M., and Breljak, D. (2011). Molecular basis of amyotrophic lateral sclerosis. Prog. Neuro-Psychopharmacology Biol. Psychiatry *35*, 370–372.

Liu, W., Wei-LaPierre, L., Klose, A., Dirksen, R.T., and Chakkalakal, J. V (2015a). Inducible depletion of adult skeletal muscle stem cells impairs the regeneration of neuromuscular junctions. Elife *4*.

Liu, W., Klose, A., Forman, S., Paris, N.D., Wei-LaPierre, L., Cortes-Lopez, M., Tan, A., Flaherty, M., Miura, P., Dirksen, R.T., et al. (2017). Loss of adult skeletal muscle stem cells drives age-related neuromuscular junction degeneration. Elife *6*.

Loeffler, J.-P., Picchiarelli, G., Dupuis, L., and Gonzalez De Aguilar, J.-L. (2016). The Role of Skeletal Muscle in Amyotrophic Lateral Sclerosis. Brain Pathol. *26*, 227–236.

Madaro, L., Passafaro, M., Sala, D., Etxaniz, U., Lugarini, F., Proietti, D., Alfonsi, M. V, Nicoletti, C., Gatto, S., De Bardi, M., et al. (2018a). Denervation-activated STAT3-IL-6 signalling in fibro-adipogenic progenitors promotes myofibres atrophy and fibrosis. Nat Cell Biol *20*, 917–927.

Magill, C.K., Tong, A., Kawamura, D., Hayashi, A., Hunter, D.A., Parsadanian, A., Mackinnon, S.E., and Myckatyn, T.M. (2007a). Reinnervation of the tibialis anterior following sciatic nerve crush injury: A confocal microscopic study in transgenic mice. Exp. Neurol. *207*, 64–74.

Majounie, E., Renton, A.E., Mok, K., Dopper, E.G.P., Waite, A., Rollinson, S., Chiò, A., Restagno, G., Nicolaou, N., Simon-Sanchez, J., et al. (2012). Frequency of the C9orf72 hexanucleotide repeat expansion in patients with amyotrophic lateral sclerosis and frontotemporal dementia: A cross-sectional study. Lancet Neurol. *11*, 323–330.

Marcuzzo, S., Zucca, I., Mastropietro, A., de Rosbo, N.K., Cavalcante, P., Tartari, S., Bonanno, S., Preite, L., Mantegazza, R., and Bernasconi, P. (2011). Hind limb muscle atrophy precedes cerebral neuronal degeneration in G93A-SOD1 mouse model of amyotrophic lateral sclerosis: A longitudinal MRI study. Exp. Neurol. *231*, 30–37.

Mathis, S., Couratier, P., Julian, A., Corcia, P., and Le Masson, G. (2017). Current view and perspectives in amyotrophic lateral sclerosis. Neural Regen. Res. *12*, 181.

Menorca, R.M.G., Fussell, T.S., and Elfar, J.C. (2013). Nerve physiology. Mechanisms of injury and recovery. Hand Clin. *29*, 317–330.

De Micheli, A.J., Laurilliard, E.J., Heinke, C.L., Ravichandran, H., Fraczek, P., Soueid-Baumgarten, S., De Vlaminck, I., Elemento, O., and Cosgrove, B.D. (2020). Single-Cell Analysis of the Muscle Stem Cell Hierarchy Identifies Heterotypic Communication Signals Involved in Skeletal Muscle Regeneration. Cell Rep. *30*, 3583-3595.e5.

Miller, R.G., Mitchell, J.D., Lyon, M., and Moore, D.H. (2007). Riluzole for amyotrophic lateral sclerosis (ALS)/motor neuron disease (MND). Cochrane Database Syst. Rev.

Mirra, A., Rossi, S., Scaricamazza, S., DI Salvio, M., Salvatori, I., Valle, C., Rusmini, P., Poletti, A., Cestra, G., Carrì, M.T., et al. (2017). Functional interaction between FUS and SMN underlies SMA-like splicing changes in wild-type hFUS mice. Sci. Rep. *7*, 1–14.

Mozzetta, C., Consalvi, S., Saccone, V., Tierney, M., Diamantini, A., Mitchell, K.J., Marazzi, G., Borsellino, G., Battistini, L., Sassoon, D., et al. (2013). Fibroadipogenic progenitors mediate the ability of HDAC inhibitors to promote regeneration in dystrophic muscles of young, but not old Mdx mice. EMBO Mol. Med. *5*, 626–639.

Muñoz-Cánoves, P., and Serrano, A.L. (2015). Macrophages decide between regeneration and fibrosis in muscle. Trends Endocrinol. Metab. *26*, 449–450.

Nishijo, K., Hosoyama, T., Bjornson, C.R.R., Schaffer, B.S., Prajapati, S.I., Bahadur, A.N., Hansen, M.S., Blandford, M.C., McCleish, A.T., Rubin, B.P., et al. (2009). Biomarker system for studying muscle, stem cells, and cancer in vivo. FASEB J. *23*, 2681–2690.

Oprescu, S.N., Yue, F., Qiu, J., Brito, L.F., and Kuang, S. (2020). Temporal Dynamics and Heterogeneity of Cell Populations during Skeletal Muscle Regeneration. IScience *23*.

Pallafacchina, G., Blaauw, B., and Schiaffino, S. (2013). Role of satellite cells in muscle growth and maintenance of muscle mass. Nutr. Metab. Cardiovasc. Dis. *23*, S12–S18.

Pasut, A., Jones, A.E., and Rudnicki, M.A. (2013). Isolation and culture of individual myofibers and their satellite cells from adult skeletal muscle. J. Vis. Exp. 50074.

Pawlikowski, B., Betta, N.D., Elston, T., Rourke, R.O., Olwin, B.B., O'Rourke, R., Jones, K., and Olwin, B.B. (2019). A cellular atlas of skeletal muscle regeneration and aging. BioRxiv 635805.

Pérez-García, M.J., and Burden, S.J. (2012). Increasing MuSK Activity Delays Denervation and Improves Motor Function in ALS Mice. Cell Rep. *2*, 497–502.

Personius, K.E., and Sawyer, R.P. (2005). Terminal Schwann cell structure is altered diaphragm of mdx mice. Muscle and Nerve *32*, 656–663.

Reddy, L. V., Koirala, S., Sugiura, Y., Herrera, A.A., and Ko, C.P. (2003). Glial cells maintain synaptic structure and function and promote development of the neuromuscular junction in vivo. Neuron *40*, 563–580.

Robert, A., and Jirounek, P. (1994). Uptake of potassium by nonmyelinating Schwann cells induced by axonal activity. J. Neurophysiol. *72*, 2570–2579.

Rosen, D.R., Siddique, T., Patterson, D., Figlewicz, D.A., Sapp, P., Hentati, A., Donaldson, D., Goto, J., O'Regan, J.P., Deng, H.X., et al. (1993). Mutations in Cu/Zn superoxide dismutase gene are associated with familial amyotrophic lateral sclerosis. Nature *362*, 59–62.

Rowland, L.P., and Shneider, N.A. (2001). Amyotrophic Lateral Sclerosis. N. Engl. J. Med. *344*, 1688–1700.

Samuel, M.A., Valdez, G., Tapia, J.C., Lichtman, J.W., and Sanes, J.R. (2012). Agrin and Synaptic Laminin Are Required to Maintain Adult Neuromuscular Junctions. PLoS One *7*.

Sandri, M., Sandri, C., Gilbert, A., Skurk, C., Calabria, E., Picard, A., Walsh, K., Schiaffino, S., Lecker, S.H., and Goldberg, A.L. (2004). Foxo transcription factors induce the atrophy-related ubiquitin ligase atrogin-1 and cause skeletal muscle atrophy. Cell *117*, 399–412.

Schiaffino, S., and Reggiani, C. (2011). Fiber types in Mammalian skeletal muscles. Physiol. Rev. *91*, 1447–1531.

Seddon, H.J. (1943). Three types of nerve injury. Brain *66*, 237–288.

Stoll, G., and Müller, H.W. (2006). Nerve Injury, Axonal Degeneration and Neural Regeneration: Basic Insights. Brain Pathol. *9*, 313–325.

Stoll, G., Griffin, J.W., Li, C.Y., and Trapp, B.D. (1989). Wallerian degeneration in the peripheral nervous system: participation of both Schwann cells and macrophages in myelin degradation. J. Neurocytol. *18*, 671–683.

Taveggia, C., Zanazzi, G., Petrylak, A., Yano, H., Rosenbluth, J., Einheber, S., Xu, X., Esper, R.M., Loeb, J.A., Shrager, P., et al. (2005). Neuregulin-1 type III determines the ensheathment fate of axons. Neuron *47*, 681–694.

Therrien, M., Dion, P.A., and Rouleau, G.A. (2016). ALS: Recent Developments from Genetics Studies. Curr. Neurol. Neurosci. Rep. *16*.

Tierney, M.T., Aydogdu, T., Sala, D., Malecova, B., Gatto, S., Puri, P.L., Latella, L., and Sacco, A. (2014). STAT3 signaling controls satellite cell expansion and skeletal muscle repair. Nat. Med. *20*, 1182–1186.

Tierney, M.T., Gromova, A., Sesillo, F.B., Sala, D., Spenlé, C., Orend, G., and Sacco, A. (2016). Autonomous Extracellular Matrix Remodeling Controls a Progressive Adaptation in Muscle Stem Cell Regenerative Capacity during Development. Cell Rep. *14*, 1940–1952.

Tiwari, N., Pataskar, A., Péron, S., Thakurela, S., Sahu, S.K., Figueres-Oñate, M., Marichal, N., López-Mascaraque, L., Tiwari, V.K., and Berninger, B. (2018). Stage-Specific Transcription Factors Drive Astrogliogenesis by Remodeling Gene Regulatory Landscapes. Cell Stem Cell *23*, 557-571.e8.

Traynor, K. (2017). FDA approves edaravone for amyotrophic lateral sclerosis. Am. J. Health. Syst. Pharm. *74*, 868.

Valdez, G., Tapia, J.C., Kang, H., Clemenson, G.D., Gage, F.H., Lichtman, J.W., and Sanes, J.R. (2010). Attenuation of age-related changes in mouse neuromuscular synapses by caloric restriction and exercise. Proc. Natl. Acad. Sci. U. S. A. *107*, 14863–14868.

Verkhratsky, A., and Butt, A. (2013). Peripheral Glial Cells. In Glial Physiology and Pathophysiology, (Chichester, UK: John Wiley & Sons, Ltd), pp. 381–430.

Wen, Y., Bi, P., Liu, W., Asakura, A., Keller, C., and Kuang, S. (2012). Constitutive Notch Activation Upregulates Pax7 and Promotes the Self-Renewal of Skeletal Muscle Satellite Cells. Mol. Cell. Biol. *32*, 2300–2311.

Wong, M., and Martin, L.J. (2010). Skeletal muscle-restricted expression of human SOD1 causes motor neuron degeneration in transgenic mice. Hum. Mol. Genet. *19*, 2284–2302.

Wosczyna, M.N., and Rando, T.A. (2018). A Muscle Stem Cell Support Group: Coordinated Cellular Responses in Muscle Regeneration. Dev Cell *46*, 135–143.

Wosczyna, M.N., Konishi, C.T., Perez Carbajal, E.E., Wang, T.T., Walsh, R.A., Gan, Q., Wagner, M.W., and Rando, T.A. (2019). Mesenchymal Stromal Cells Are Required for Regeneration and Homeostatic Maintenance of Skeletal Muscle. Cell Rep. *27*, 2029-2035.e5.

Yu, B., and Pamphlett, R. (2017). Environmental insults: Critical triggers for amyotrophic lateral sclerosis. Transl. Neurodegener. *6*, 15.

Yu, W.M., Yu, H., Chen, Z.L., and Strickland, S. (2009). Disruption of laminin in the peripheral nervous system impedes nonmyelinating schwann cell development and impairs nociceptive sensory function. Glia *57*, 850–859.

Yusuf, F., and Brand-Saberi, B. (2012). Myogenesis and muscle regeneration. Histochem. Cell Biol. *138*, 187–199.

Zeng, T., and Dai, H. (2019). Single-cell RNA sequencing-based computational analysis to describe disease heterogeneity. Front. Genet. *10*.

Zhu, H., Xiao, F., Wang, G., Wei, X., Jiang, L., Chen, Y., Zhu, L., Wang, H., Diao, Y., Wang, H., et al. (2016). STAT3 Regulates Self-Renewal of Adult Muscle Satellite Cells during Injury-Induced Muscle Regeneration. Cell Rep. *16*, 2102–2115.

8. LIST OF PUBLICATIONS

Proietti D, Giordani L, De Bardi M, Lozanoska-Ochser B, Amadio S, Volontè C, Marinelli S, Muchir A, Bouchè M, Borsellino G, Sacco A, Puri PL and Madaro L. "Activation of muscle-resident glial cells by nerve injury" *Under review, JCI Insight*
Impact Factor: 6.014 (2018)

Vacca V, Madaro L, De Angelis F, **Proietti D**, Cobianchi S, Orsini T, Puri PL, Luvisetto S, Pavone F and Marinelli S. "Revealing the Therapeutic Potential of Botulinum Neurotoxin Type A in Counteracting Paralysis and Neuropathic Pain in Spinally Injured Mice" *Toxins* 2020, *12*(8), 491; https://doi.org/10.3390/toxins12080491
Impact Factor: 3.273 (2019/2020)

Scaricamazza S, Salvatori I, Giacovazzo G, Philippe Loeffler J, Renè F, Rosina M, Quessada C, **Proietti D**, Heil C, Rossi S, Battistini S, Giannini F, Volpi N, Frederik J. Steyn, Shyuan T. Ngo., Ferraro E, Madaro L, Coccurello R, Valle C and Ferri A. "Skeletal-muscle metabolic reprogramming in ALS-SOD1^{G93A} mice predates disease onset and is a promising therapeutical target" *iScience*. 2020 May 22;23(5):101087. doi:10.1016/j.isci.2020.101087. Epub 2020 Apr 21.
Impact Factor: 4.447 (2019)

Biferali B, **Proietti D**, Mozzetta C, and Madaro L. "Fibro–Adipogenic Progenitors Cross-Talk in Skeletal Muscle: The Social Network." *Front. Physiol*. 2019. *10*, 1074. doi: 10.3389/fphys.
Impact Factor: 4.134 (2019)

Apolloni S, Amadio S, Fabbrizio P, Morello G, Spampinato AG, Latagliata EC, et al. Histaminergic transmission slows progression of amyotrophic lateral sclerosis. *J Cachexia Sarcopenia Muscle*. 2019; jcsm.12422 doi: 10.1002/jcsm.12422
Impact Factor: 12.511(2018)

Bouchè M, Lozanoska-Ochser B, **Proietti D**, Madaro L. Do neurogenic and cancer-induced muscle atrophy follow common or divergent paths? *Eur J Transl Myol*. 2018; 28(4):7931. doi: 10.4081/ejtm.2018.7931

Madaro L, Passafaro M, Sala D, Etxaniz U, Lugarini F, **Proietti D**, Alfonsi MV, Nicoletti C, Gatto S, De Bardi M, Rojas-García R, Giordani L, Marinelli S, Pagliarini V, Sette C, Sacco A, Puri PL. "Denervation-activated STAT3-IL-6 signalling in fibro-adipogenic progenitors promotes myofibres atrophy and fibrosis." *Nat. Cell Biol*. 2018 20(8), 917-927. doi: 10.1038/s41556-018-0151-y
Impact Factor: 20.042 (2019)

D'Agostino M, Torcinaro A, Madaro L, Beji S, Marchetti L, Sileno S, Salis C, **Proietti D**, Imeneo G, Capogrossi MC, De Santa F and Magenta A "Role of miR-200c in myogenic differentiation impairment via p66Shc: implication in skeletal muscle regeneration of dystrophic mdx mice". *Oxidative Medicine and Cellular Longevity* 2018. doi: 10.1155/2018/4814696
Impact Factor: 5.076